CANCER

Multiepitope supramolecular peptide nanofibers eliciting coordinated humoral and cellular antitumor immune responses

Yaoying Wu[1], Hanning Wen[1], Zachary J. Bernstein[1], Kelly M. Hainline[1], Tykia S. Blakney[1], Kendra L. Congdon[2], David J. Snyder[2], John H. Sampson[2], Luis Sanchez-Perez[2], Joel H. Collier[1]*

Subunit vaccines inducing antibodies against tumor-specific antigens have yet to be clinically successful. Here, we use a supramolecular α-helical peptide nanofiber approach to design epitope-specific vaccines raising simultaneous B cell, CD8+ T cell, and CD4+ T cell responses against combinations of selected epitopes and show that the concurrent induction of these responses generates strong antitumor effects in mice, with significant improvements over antibody or CD8+ T cell–based vaccines alone, in both prophylactic and therapeutic subcutaneous melanoma models. Nanofiber vaccine–induced antibodies mediated in vitro tumoricidal antibody-dependent cellular cytotoxicity (ADCC) and antibody-dependent cellular phagocytosis (ADCP). The addition of immune checkpoint and phagocytosis checkpoint blockade antibodies further improved the therapeutic effect of the nanofiber vaccines against murine melanoma. These findings highlight the potential clinical benefit of vaccine-induced antibody responses for tumor treatments, provided that they are accompanied by simultaneous CD8+ and CD4+ responses, and they illustrate a multiepitope cancer vaccine design approach using supramolecular nanomaterials.

INTRODUCTION

Tumor-specific antibodies produced either endogenously or exogenously are promising anticancer therapeutics, but their efficacy has been limited when used in isolation. High levels of endogenous tumor-specific antibody responses are associated with favorable prognoses in cancer patients (1–5), promoting tumor cell killing in part by natural killer (NK) cells via antibody-dependent cellular cytotoxicity (ADCC) (6). Monoclonal antibodies (mAbs) against tumor-associated antigens (TAAs), including epidermal growth factor receptor (EGFR) (7) and HER2 receptors (8), have been developed to induce this antibody-mediated tumor cell killing. In addition to mediating ADCC and antibody-dependent cellular phagocytosis (ADCP), TAA-specific antibodies can facilitate T cell immunity by improving the presentation of additional antigens and reprogramming the tumor microenvironment via the elicitation of inflammatory chemokines and cytokines (9–11). Further, the combination of TAA-specific antibody therapies with additional treatment modalities has shown promise; for example, a combined immunotherapy consisting of a CD8+ T cell vaccine, Interleukin-2 (IL-2), and anti–programmed death ligand 1 (aPD-L1) was shown to be capable of eliminating large tumor burdens in mice (9). Notably, the therapeutic efficacy was significantly diminished when the TAA-specific mAbs were eliminated from the combination therapy, suggesting a synergy between CD8+ T cells and the tumor-specific antibodies. Nevertheless, mAb therapies continue to be limited by antidrug immune responses, high cost, and associated toxicity (12–14).

Peptide-based cancer vaccines aiming to generate tumor-specific CD8+ T cells that ultimately lead to tumor lysis (15) have seen dramatic improvements in recent years (16–19). Contrastingly, humoral vaccines that raise antibodies against tumor surface antigens, such

as the tumor-specific EGFR variant III (EGFRvIII), have thus far shown little long-term survival benefit in clinical trials (20, 21). The poor clinical responses to humoral cancer vaccines have been attributed in part to immunological escape by tumor cells via reduced target expression (22–24). Similar adaptive resistance has also been observed in other single-target treatments (25–28). These limitations highlight an urgent need to design combination immunotherapies capable of generating therapeutic responses complimentary to antibodies to minimize the potential for immunological escape. Considering the demonstrated therapeutic synergy between TAA-specific mAbs and CD8+ T cell vaccines (9), we envision that a peptide vaccine stimulating simultaneous CD8+ T cell responses and antibody responses against multiple different selected tumor antigens could be advantageous.

B cell peptide antigens are often poorly immunogenic and thus need to be conjugated onto delivery platforms to induce humoral responses (29). However, conventional carrier systems have limited ability for combining multiple different peptide epitopes and adjusting the relative amounts of each. We recently developed a peptide nanofiber vaccine platform based on the 29-mer α-helical self-assembling peptide Coil29 (QARILEADAEILRAYARILEAHAEILRAD) (Fig. 1A) and demonstrated its ability to elicit peptide epitope–specific humoral responses with antibody titers and affinities superior to other adjuvants including Alum, Sigma Adjuvant System (SAS), and Complete Freund's Adjuvant (CFA) (30, 31). In addition, Coil29 nanofibers bearing model CD8+ T cell epitopes have been shown to generate antigen-specific CD8+ T cell responses comparable to peptide/CFA emulsions (30). The Coil29 platform can carry a wide range of peptide antigens via peptide N-terminal modifications while retaining the ability to self-assemble into α-helical nanofibers (30–32). The modularity of this self-assembling system enables the facile simultaneous delivery of multiple peptide antigens by co-assembling multiple epitope-carrying peptides into a single nanofiber. For these reasons, Coil29 is a useful platform for delivering both B cell and T cell peptide epitopes to elicit simultaneous humoral and cellular immune responses.

[1]Department of Biomedical Engineering, Duke University, Durham, NC, USA.
[2]Department of Neurosurgery, Duke University, Durham, NC, USA.
*Corresponding author. Email: joel.collier@duke.edu
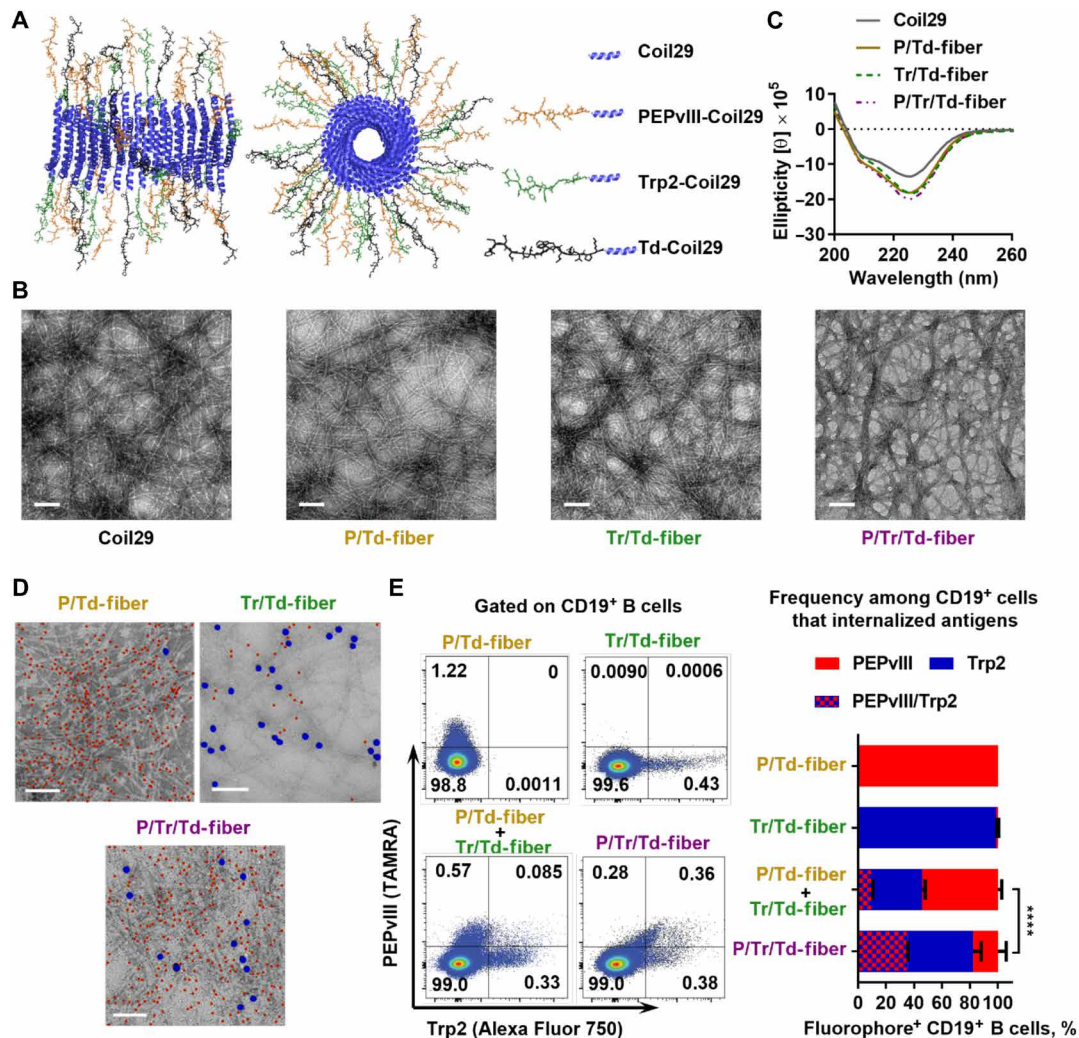
Fig. 1. Co-assembled Coil29 peptides exhibit fibril morphologies and deliver both B cell and T cell peptide epitopes simultaneously. (**A**) Schematics of α-helical Coil29 nanofiber carrying multiple epitopes, drawn using Protein Data Bank (PDB) structures for Coil29 (PDB ID 3J89). Left, side view; right, axial view. (**B**) All assemblies exhibited similar α-helical secondary structures by CD, consistent with unmodified Coil29. (**C**) Multiepitope Coil29 nanofibers exhibited fibrillar morphologies similar to unmodified Coil29 by TEM. Scale bar, 100 nm. (**D**) Representative immunogold-labeled TEM images indicate that co-assembled nanofibers presented both Trp2 (5 nm) and PEPvIII (10 nm) epitopes Scale bar, 100 nm. Five-nanometer particles (PEPvIII labeling) are false-colored red, and 10-nm particles (Trp2 labeling) are false-colored blue for clarity. (**E**) Uptake of assembled fluorophore-labeled peptides (TAMRA-PEPvIII-Coil29 and Alexa Fluor 750–Trp2–Coil29) by CD19^{+} B cells 4 hours after intraperitoneal administration of either single fluorophore-labeled nanofibers (PE or Alexa Fluor 750) or two fluorophore-labeled co-assembled nanofibers (PE/Alexa Fluor 750) confirmed co-assembly between Trp2-Coil29 and PEPvIII-Coil29 peptides. Left, representative flow histograms; right, percentage of B cells internalizing either or both fluorophores among the fluorophore-positive B cells. (****$P < 0.0001$ by χ^2 test, $N = 3$).

In the present work, a multiepitope antitumor vaccine was investigated by co-assembling Coil29 peptides carrying PEPvIII (LEEKKGNYVVTDH), a B cell peptide epitope against EGFRvIII receptors (20, 33), and Trp2 (SVYDFFVWL), a melanoma-associated CD4^{+} T cell peptide antigen (34). Although the Coil29 assembly domain already contains identified CD4^{+} T cell epitopes (31), to provide additional tumor-specific CD4^{+} T cell help for enhancing humoral and cellular immune responses (35–37), we additionally incorporated the tetanus toxoid CD4^{+} T cell epitope (Td) (38) (FNNFTVSFWLRVPKVSASHLE) into the co-assembled Coil29 nanofibers. Epitope-bearing Coil29 nanofibers elicited PEPvIII-specific antibodies and Trp2-specific CD8^{+} T cell responses, with help from platform-directed CD4^{+} T cell responses, collectively enhancing tumor rejection in both prophylactic and therapeutic EGFRvIII-expressing melanoma models. Therapeutic efficacy could be enhanced further by combination with immune checkpoint (aPD-L1) (39) and phagocytosis checkpoint (aCD47) (40, 41) blockade antibodies. This study offers a strategy for enhancing the antitumor functions of vaccine-induced antibodies, generates insight into the therapeutic synergy between humoral and cellular antitumor responses, and provides a supramolecular design strategy for combination cancer vaccines.

RESULTS

Co-assembled peptide nanofibers deliver multiple epitopes simultaneously

We first synthesized and purified epitope-bearing Coil29 peptides, including PEPvIII-Coil29 (B cell epitope), Trp2-Coil29 (CD8+ T cell epitope), and Td-Coil29 (CD4+ T cell epitope) (table S1) and examined their co-assembly behavior. To investigate the role of humoral and cellular immune responses in vivo, we co-assembled epitope-bearing peptides in phosphate-buffered saline (PBS) at the indicated molar ratio to yield Coil29 nanofibers carrying B cell epitopes [P/Td-fiber (PEPvIII-Coil29:Td-Coil29:Coil29 = 1:1:1)], CD8+ T cell epitopes [Tr/Td-fiber (Trp2-Coil29:Td-Coil29:Coil29 = 1:1:1)], or both B cell and CD8+ T cell epitopes [P/Tr/Td-fiber (PEPvIII-Coil29:Trp2-Coil29:Td-Coil29 = 1:1:1)] (Fig. 1A). By transmission electron microscopy (TEM) imaging, the morphologies of the multiepitope nanofibers resembled unmodified Coil29 nanofibers (Fig. 1B), and circular dichroism (CD) further verified that the α-helical secondary structure was preserved across all four formulations, as evidenced by the double absorbance minima at 208 and 222 nm (Fig. 1C). Consistent with previous findings (30, 31), Coil29 nanofibers were capable of being appended with the various peptide epitopes while maintaining their morphology and secondary structure.

To confirm the assembly and presentation of Trp2 and PEPvIII epitopes along the Coil29 nanofibers, we visualized them using immunogold labeling and TEM. PEPvIII-Coil29 and Trp2-Coil29 were functionalized with azodibenzocyclooctyne (DBCO) and biotin, respectively, and visualized with gold nanoparticles functionalized with azide (5 nm) or streptavidin (10 nm) (Fig. 1D and fig. S1) (42). The co-assembled P/Tr/Td-fibers bound both nanoparticles, whereas P/Td-fiber primarily bound cognate 5-nm gold particles and Tr/Td-fibers primarily bound cognate 10-nm nanoparticles, although low levels of off-target background staining common to this technique were also observed (43). To determine whether P/Td-fibers were co-assembled, rather than being a mixture of P/Td-fiber and Tr/Td-fiber, we measured the in vivo cellular uptake of fluorophore-labeled nanofibers, where PEPvIII-Coil29 peptides were labeled with TAMRA and Trp2-Coil29 peptides were labeled with Alexa Fluor 750. Mice were intraperitoneally administered either a mixture of P/Td-fiber and Tr/Td-fiber or the co-assembled P/Tr/Td-fiber, with P/Td-fiber and Tr/Td-fiber alone as controls. Peritoneal lavage fluid was collected 4 hours later, and labeled nanofiber uptake was evaluated (Fig. 1E and fig. S2). Among antigen-fluorophore–positive cells, 35.3% of nanofiber-internalized CD19+ B cells took up both fluorophores when P/Tr/Td-fibers were administered. However, when P/Td-fibers and Tr/Td-fibers were delivered separately, only 9.9% CD19+ B cells were positive for both fluorophores, and most cells only internalized either P/Td-fibers (54.3%) or Tr/Td-fibers (35.8%). Administration of nanofibers labeled only with either P/Td-fibers (TAMRA) or Tr/Td-fibers (Alexa Fluor 750) yielded single-color positive B cells as expected. It is worth noting that we focus on CD19+ B cells for our analysis here because nanofibers were predominantly taken up by CD19+ B cells in the mouse peritoneal cavity, whereas F4/80+ macrophages and CD11c+MHCII+ dendritic cells (DCs) internalized smaller percentages of fluorophore-labeled nanofibers at this site (fig. S2). This uptake experiment corroborated the nanogold-labeled TEM images and further suggested that a significant proportion of P/Tr/Td-fibers carried both B cell and CD8+ T cell epitopes.

We next assessed whether CD4+ and CD8+ T cell epitopes can be efficiently processed when delivered by co-assembled nanofibers using DOBW (44) and B3Z (18) assays (fig. S3). We synthesized a SIINFEKL-Coil29 peptide bearing the CD8+ T cell epitope OVA$_{257-264}$ and an OVA$_{323-339}$-Coil29 peptide and formulated single-epitope nanofibers and co-assembled SIINFEKL/OVA$_{323-339}$-fibers. Bone marrow–derived DCs (BMDCs) were incubated with nanofibers at various epitope concentrations (0.03 to 31.2 nM) for 4 hours, after which reporter hybridoma cell lines were applied to detect the epitope presentation levels. For both CD8+ epitope presentation (B3Z) and CD4+ epitope presentation (DOBW), co-assembled nanofibers (SIINFEKL/OVA$_{323-339}$-fiber) exhibited a similar, if not better, ability to mediate antigen presentation as compared to single epitope-carrying nanofibers (SIINFEKL-fiber or OVA$_{323-339}$-fiber) in the peptide concentration range tested. In addition, all nanofibers were more effective in mediating antigen presentation than nonassembled soluble peptides alone. This demonstrated that CD4+ and CD8+ T cell epitopes delivered by co-assembled nanofibers could be efficiently internalized and presented by DCs.

Co-assembled P/Tr/Td-fibers generate strong humoral responses

We have previously demonstrated that nanofiber vaccines carrying both B cell epitopes and CD4+ T cell epitopes can induce strong antigen-specific humoral responses (31). To examine whether the added CD8+ T cell epitope influenced immunogenicity, we monitored the long-term PEPvIII-specific immunoglobulin G (IgG) titers in C57BL/6 mice after receiving three immunizations (weeks 0, 2, and 4) with P/Td-fibers or P/Tr/Td-fibers (Fig. 2A). For comparison, we also immunized mice with CFA emulsions containing all three peptide epitopes (PEPvIII, Trp2, and Td). We selected CFA owing to its strong immunostimulatory properties, although CFA is not acceptable for use in humans (45). Immunization with nanofibers alone typically yields T helper 2 (T$_H$2)–biased IgG responses (30, 35), so to generate T$_H$1-biased humoral responses for antitumor efficacy, we additionally used CpG, a Toll-like receptor 9 (TLR9) agonist (46–48), as an adjuvant in all nanofiber formulations described hereafter. Both P/Td-fibers and P/Tr/Td-fibers stimulated strong and durable PEPvIII-specific IgG responses over 21 weeks, with a peak log$_{10}$ titer of 3.75 for P/Tr/Td-fiber and 3.25 for P/Td-fiber on week 7 (Fig. 2A). Responses elicited by P/Td-fibers waned slightly over time and decreased to an average titer of 2.5 by week 21, but the IgG log$_{10}$ titers of mice receiving P/Tr/Td-fiber immunizations were comparatively stable. The differences between the two nanofibers were not statistically significant, indicating that the incorporation of Trp2 epitopes in P/Tr/Td-fiber did not impair its ability to stimulate PEPvIII-specific IgG responses. The addition of CpG adjuvant also increased IgG2b responses, suggesting a skewing toward T$_H$1-biased humoral responses against nanofibers (fig. S4). CFA emulsions raised poor IgG antibodies against PEPvIII peptides, with a peak average titer of 1.75 on week 5 and antibody concentration declining to near baseline by 15 weeks. To evaluate humoral immune memory in immunized mice, one additional vaccination was given on week 22. IgG concentrations were significantly elevated in all three groups 7 days later, with P/Tr/Td-fiber group yielding the highest log$_{10}$ titers of 4.75. The rapid recall responses suggested anti-PEPvIII humoral memory in all three immunization groups. To examine the specificity of the elicited IgG antibodies, we pooled sera collected between week 5 and week 10 from mice in Fig. 2A, applied them to either B16vIII (EGFRvIII-expressing B16F10 cells) or B16F10 (negative control cells) for 30 min, and then stained the sera-treated cells with
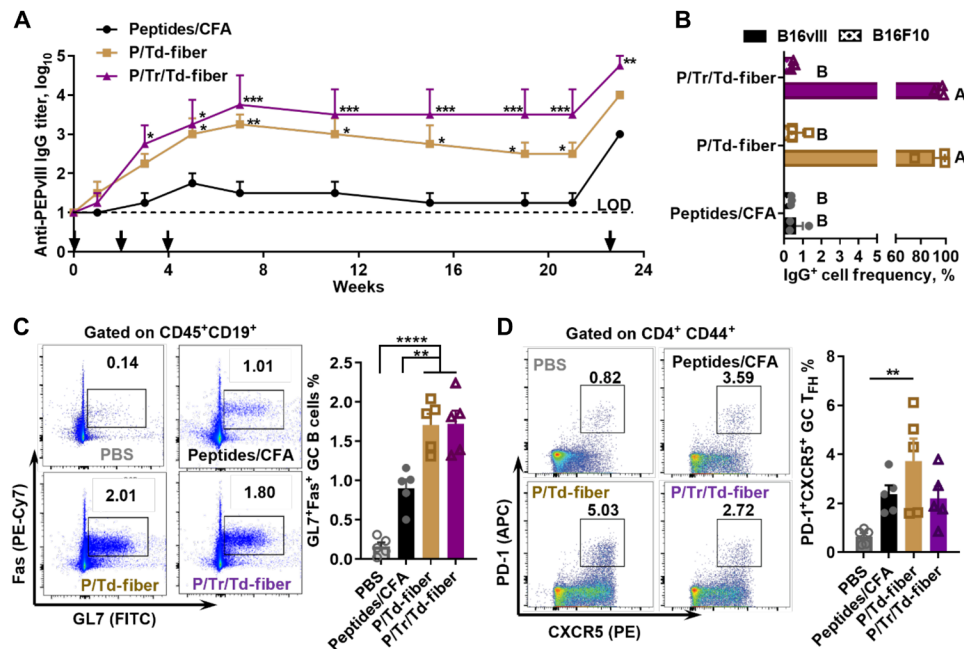
Fig. 2. Multiepitope nanofibers generate strong antigen-specific humoral responses with high frequencies of GC B cells and T_{FH} cells. (**A**) P/Tr/Td-fiber and P/Td-fiber both generated long-lasting PEPvIII-specific IgG responses after three subcutaneous immunizations, and humoral memory could be recalled after immunization on week 22. Dashed line represents limit of detection (LOD). Asterisks indicate statistical significance compared to peptide/CFA emulsion group, calculated through multiple comparison by two-way ANOVA with Tukey test, $N = 4$ (*$P < 0.05$, **$P < 0.01$, ***$P < 0.001$, and ****$P < 0.0001$). (**B**) IgG antibodies in sera from mice immunized with nanofibers efficiently bind to EGFRvIII receptors on B16vIII cells (sera pooled from week 5 to week 10). Groups not sharing letters are statistically different ($P < 0.0001$, by multiple comparison through two-way ANOVA with Tukey test, $N = 3$). (**C**) Frequencies of GC B cells (FVD-CD45$^+$CD19$^+$GL7$^+$Fas$^+$) in draining lymph nodes 7 days after the second subcutaneous immunization. Asterisks stand for statistical significances by multiple comparison calculated using one-way ANOVA with Tukey test, $N = 5$. Left, representative flow histograms; right, data summary. (**D**) Frequencies of GC T_{FH} cells (FVD-CD3e$^+$CD4$^+$CD44$^+$CXCR5$^+$PD-1$^+$) in draining lymph nodes 7 days after second immunizations. Statistical difference was determined by multiple comparison using one-way ANOVA with Tukey test. $N = 5$, $P = 0.0033$. Left, representative flow histograms; right, data summary.

fluorescein isothiocyanate (FITC)–anti-IgG antibodies (Fig. 2B). In total, 95.4% of P/Tr/Td-fiber sera-treated B16vIII cells and 91.1% of P/Td-fiber sera-treated B16vIII cells were IgG positive, but less than 1% of B16F10 cells were decorated with IgG from any group, suggesting that specific EGFRvIII-binding antibodies had been raised. In contrast, CFA-adjuvanted peptides did not raise a significant amount of IgG antibodies binding either B16vIII or B16F10 cells. Therefore, compared to CFA emulsions, both P/Tr/Td-fibers and P/Td-fibers were more efficient in generating IgG responses against the peptide antigen, PEPvIII, with P/Tr/Td-fibers eliciting slightly higher titers of IgG responses.

With nanofibers generating higher $\log_{10}$ titers of antibodies than CFA emulsions, we hypothesized that the nanofiber vaccine could induce strong germinal center (GC) responses (*49*). To test this hypothesis, we harvested draining lymph nodes 7 days after the second immunizations and analyzed GC B cell frequencies (CD45$^+$CD19$^+$ GL7$^+$Fas$^+$). Both P/Td-fibers and P/Tr/Td-fibers stimulated similar levels of GC B cells, 1.68% and 1.72%, respectively, among all B cells (Fig. 2C). In comparison, CFA immunization yielded significantly lower frequencies of GC B cells, only 0.90% among all B cells ($P < 0.01$). The difference in GC responses elicited by the three groups is consistent with the long-term antibody responses discussed above. Seeking to understand the difference in humoral immunogenicity between nanofibers and CFA emulsions, we further examined follicular T helper (T_{FH}) cell frequency elicited by nanofiber vaccines owing to the critical role of T_{FH} cells in humoral immune responses

(*50*). All three vaccines generated comparable levels of T_{FH} cell responses (CD4$^+$CD44$^+$PD-1$^+$CXCR5$^+$) 7 days after second immunizations (Fig. 2D). P/Td-fiber group showed the highest frequencies of T_{FH}, 3.73% among antigen expressing CD4$^+$ T cells (CD4$^+$CD44$^+$). A slightly lower average frequency of T_{FH} cells was found in P/Tr/Td-fiber (2.20%) and CFA groups (2.38%). Collectively, these data demonstrated that P/Tr/Td-fiber and P/Td-fibers stimulated superior GC responses and comparable levels of T_{FH} cell responses when compared to CFA emulsions.

Multiepitope nanofibers stimulate strong T cell responses

We next sought to examine the ability of P/Tr/Td-fibers to generate antigen-specific cellular responses using enzyme-linked immunospot (ELISPOT). C57BL/6 mice were immunized twice on weeks 0 and 2 with either CpG-adjuvanted nanofibers (Tr/Td-fiber or P/Tr/Td-fiber) or CFA emulsions. PBS was administered as a sham immunization. Splenocytes were harvested from mice 7 days after the second immunization to detect antigen-specific interferon-γ (IFNγ)–secreting T cells using ELISPOT assays. When stimulated with Trp2 peptides, the CD8$^+$ T cell epitope, all three groups showed equivalent levels of T cell responses, about 10 spot-forming cells (SFCs) per 0.25 M splenocytes (Fig. 3A). Similarly, stimulation with Td peptides, the CD4$^+$ T cell epitopes, yielded a comparable level of IFNγ-specific T cell responses among the three treatment groups (Fig. 3B). In addition, the P/Td-fibers exhibited a similar ability to stimulate Td-specific CD4$^+$ T cell responses (fig. S5). We also sampled
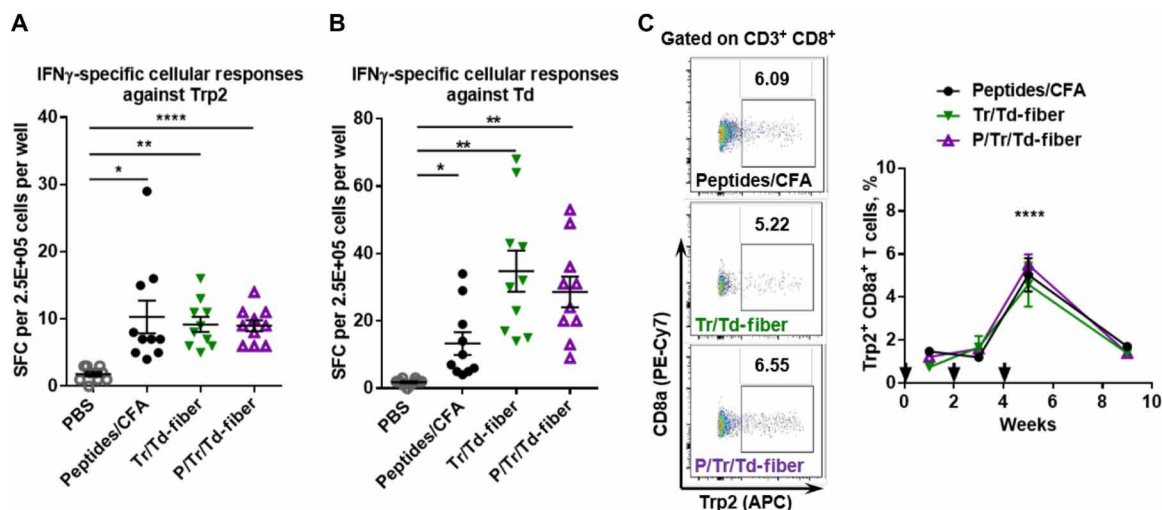
Fig. 3. Multiepitope nanofibers generate strong cellular responses against Trp2 and Td epitopes. Mice were subcutaneously immunized with indicated formulations on days 0 and 14, and splenocytes from immunized mice were harvested for IFNγ-specific ELISPOT. Both P/Tr/Td-fiber and Tr/Td-fiber generated strong IFNγ-secreting cellular responses upon stimulation with Trp2 peptides (**A**) and Td peptides (**B**) (*$P < 0.05$, **$P < 0.01$, and ****$P < 0.0001$, multiple comparison by one-way ANOVA with Dunnett test, as compared to PBS group, $N = 10$). (**C**) Mice were immunized with indicated formulations on days 0, 14, and 28. PBMCs from immunized mice were sampled on days 7, 21, 35, and 56 for the presence of Trp2-specific CD8+ T cells. Left, flow histograms; right, data summary. No statistical differences were found between different immunization groups. (****$P < 0.0001$ between day 35 and all other days within each immunization group by multiple comparison using two-way ANOVA with Tukey test, $N = 5$).

peripheral blood mononuclear cells (PBMCs) for Trp2-specific CD8+ T cells (FVD−CD3+CD8+Trp2 tetramer+) after mice received immunizations with either nanofibers or CFA emulsion to assess the magnitude and kinetics of the induced cellular responses. The frequency of Trp2+CD8+ T cells among CD8+ T cells in the three groups (CFA, Tr/Td-fiber, and P/Tr/Td-fiber) was indistinguishable over time, with the highest percentage of around 5% reached on week 5 after receiving three immunizations for all three groups (Fig. 3C). The Trp2+CD8+ T cell frequency slowly waned after week 5, as most effector CD8+ T cells are short-lived (*51*). This suggests that neither nanofibers nor CFA emulsions were effective at providing sustained stimulations for T cell activity against the Trp2 peptide antigens. Together, nanofiber vaccines, both P/Tr/Td-fiber and Tr/Td-fiber, showed similar abilities to generate antigen-specific CD8+ and CD4+ T cell responses that were as strong as those raised by CFA emulsions.
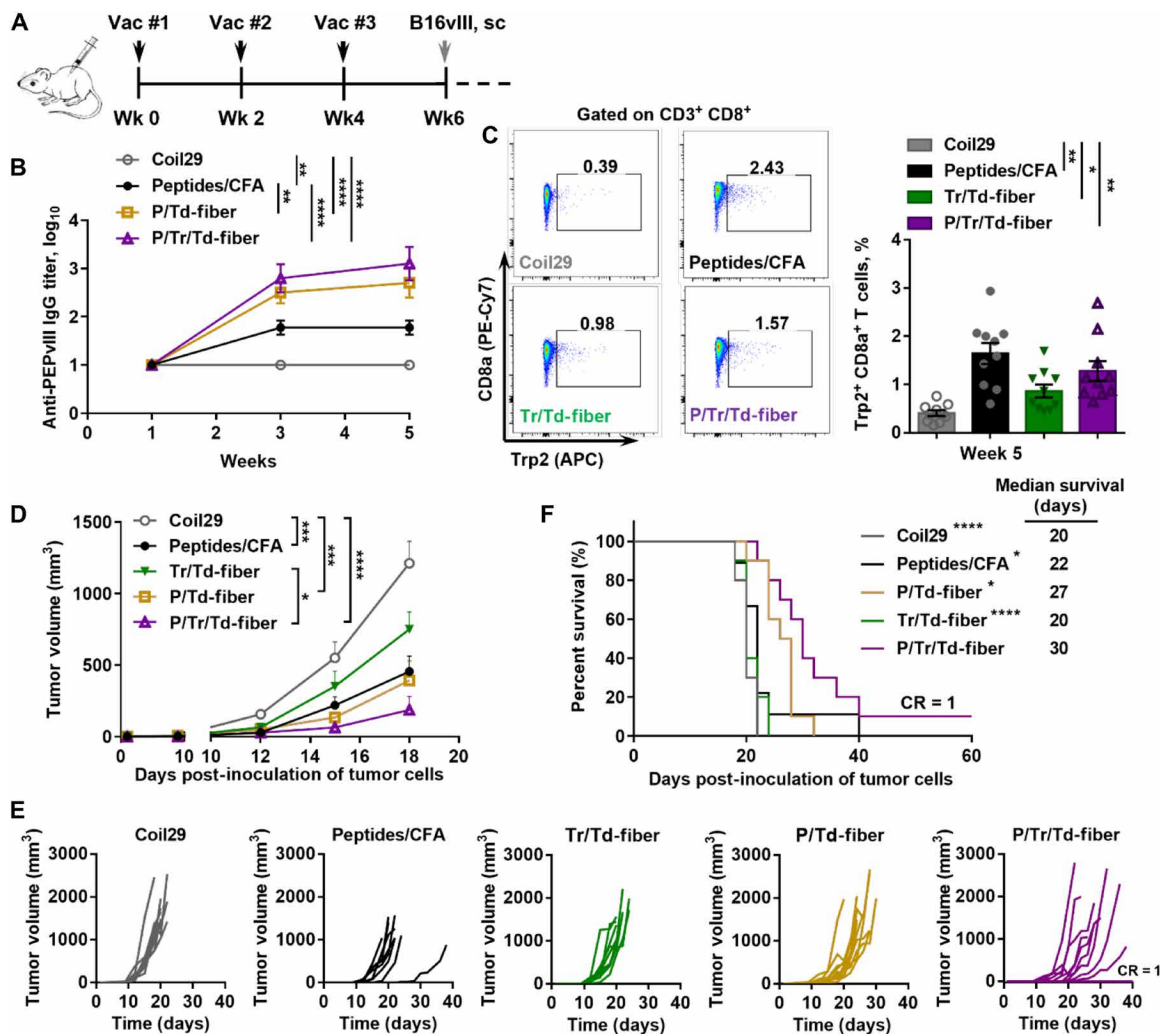
Immunizations with P/Tr/Td-fibers significantly hindered tumor growth
Having confirmed the immunogenicity of co-assembled nanofibers, we next examined the protective effects of vaccine-induced humoral and cellular immunity in a prophylactic B16vIII tumor model (Fig. 4). We first established antitumor immunity by vaccinating mice with nanofibers (P/Tr/Td-fiber, P/Td-fiber, or Tr/Td-fiber) or CFA emulsions. Unmodified Coil29 nanofibers were also included to test for any immunogenicity of nanofibers lacking TAAs. The levels of PEPvIII-specific IgG responses after three immunizations were consistent with previous findings, with both P/Tr/Td-fibers and P/Td-fibers stimulating higher titers of antibodies than CFA emulsions (Fig. 4B). P/Tr/Td-fibers also stimulated similar frequencies of Trp2-specific CD8+ T cell responses (1.28%), as compared to CFA emulsions (1.65%) and Tr/Td-fibers (0.87%) (Fig. 4C). With elicited immune responses confirmed, we challenged the immunized mice with 1×10^5 EGFRvIII-expressing B16vIII cells subcutaneously 2 weeks

after final immunizations (Fig. 4, D to F). Tumor growth was significantly delayed in mice immunized with P/Tr/Td-fibers, and P/Tr/Td-fiber immunizations improved overall survival, with 1 of 10 mice showing complete rejection (Fig. 4F). Prophylactically administered P/Td-fibers also exhibited a slight antitumor effect, suggesting that vaccine-induced antibodies can contribute to some tumor inhibition, although with less efficacy without the simultaneous T cell responses evoked by the full P/Tr/Td-fiber formulation. Although the CFA group exhibited low anti-PEPvIII titers, CFA emulsions also provided significant protection against the tumor challenge, possibly due to its ability to raise strong CD8+ T cell responses. Conversely, with only low frequencies of Trp2+CD8+ T cell responses, mice immunized with Tr/Td-fibers were unable to delay tumor growth. Individually, vaccine-induced antitumor cellular and humoral responses both demonstrated a protective benefit against tumor challenge, but efficacy was significantly improved when the two responses were simultaneously raised by the co-assembled P/Tr/Td-fibers.

Vaccination with P/Tr/Td-fibers was efficacious in a B16vIII tumor model
To examine the therapeutic efficacy of the P/Tr/Td-fiber vaccines, we treated B16vIII tumor–bearing mice with either nanofiber vaccines (P/Td-fiber, Tr/Td-fiber, or P/Tr/Td-fiber) or CFA vaccines 1 day after tumor inoculation (Fig. 5). Consistent with the prophylactic model, P/Tr/Td-fibers were able to significantly delay the tumor growth, while all other nanofiber formulations exhibited little therapeutic benefit. CFA emulsions also showed a slight therapeutic benefit in tumor growth and survival, possibly benefiting from the strong CD8+ T cell responses. These data confirmed that the CD8+ T cell and antibody responses alone were not effective in tumor treatment, but the therapeutic efficacy could be significantly improved when both cellular and humoral immunity were raised by co-assembled nanofibers.

Fig. 4. B16vIII tumor growth was significantly inhibited in mice with vaccine-induced humoral and cellular antitumor immunity stimulated by multiepitope nanofibers. (**A**) C57BL/6 mice received three subcutaneous immunizations (black arrows) and subsequently received 1×10^5 B16vIII tumor cells subcutaneously on the flank 14 days after final immunizations. PEPvIII-specific IgG titers in sera were monitored 1 week after each vaccination. (**B**) Both P/Tr/Td-fiber and P/Td-fibers stimulated strong PEPvIII-specific IgG responses after three immunizations (**$P < 0.001$ and ****$P < 0.0001$ by multiple comparison via two-way ANOVA with Tukey test, $N = 10$). (**C**) Both P/Tr/Td-fiber and Tr/Td-fiber and peptides/CFA emulsion group stimulated significant level of Trp2-specific CD8$^+$ T cells on week 5 (*$P < 0.05$ and **$P < 0.01$ by multiple comparison using one-way ANOVA with Tukey test, $N = 10$). P/Tr/Td-fiber prophylactic immunization inhibited B16vIII tumor growth (D) and improved overall survival challenges (F). (**D**) Tumor growth measured over time (*$P < 0.05$, ***$P < 0.001$, and ****$P < 0.0001$, two-way ANOVA with Tukey test, $N = 10$). (**E**) Individual tumor growth curves. (**F**) Overall survival of tumor-bearing mice and median survival (*$P < 0.05$ and ****$P < 0.0001$ compared to P/Tr/Td-fiber group by log-rank test, $N = 10$).

Combination with checkpoint blockade further improved nanofiber vaccine treatment efficacy

Although fully co-assembled nanofiber vaccines reduced tumor growth, we reasoned that the suppressive tumor microenvironment (*52*) may have limited the efficacy of P/Tr/Td-fiber vaccines. Therefore, we explored the combination of aCD47 blockade antibodies and aPD-L1 blockade antibodies to further improve the therapeutic efficacy of P/Tr/Td-fibers. The PD-L1 ligand plays a pivotal role in tumor inhibition of T cell responses, and aPD-L1 antibodies can block tumor immune resistance and enhance T cell antitumor activity (*39*). The CD47–signal regulatory protein α (SIRPα) interaction is a tumor phagocytosis checkpoint, and blockade of overexpressed CD47 receptors on tumor cells has been previously shown to enhance

both ADCC by NK cells and ADCP by macrophages (*40*, *41*, *53–55*). The therapeutic efficacy of aCD47 antibodies can be further enhanced when coadministered with TAA-specific mAbs (*53*, *54*, *56*, *57*). Here, we speculated that combining aCD47 with Coil29 nanofiber vaccines may enhance the therapeutic effect of elicited anti-PEPvIII IgG antibodies. We first examined whether vaccine-induced anti-PEPvIII humoral responses could mediate ADCC activity using flow cytometry (*58*). We cocultured splenocyte-derived NK cells (fig. S6) and carboxyfluorescein diacetate succinimidyl ester (CFSE)–labeled B16vIII cells in the presence of the sera from mice immunized either with P/Td-fibers at various dilutions or with PBS-immunized mouse sera at an effector cell:target cell (E:T) ratio of 1:1 (fig. S7). The anti-B16vIII activities showed sera concentration dependence,
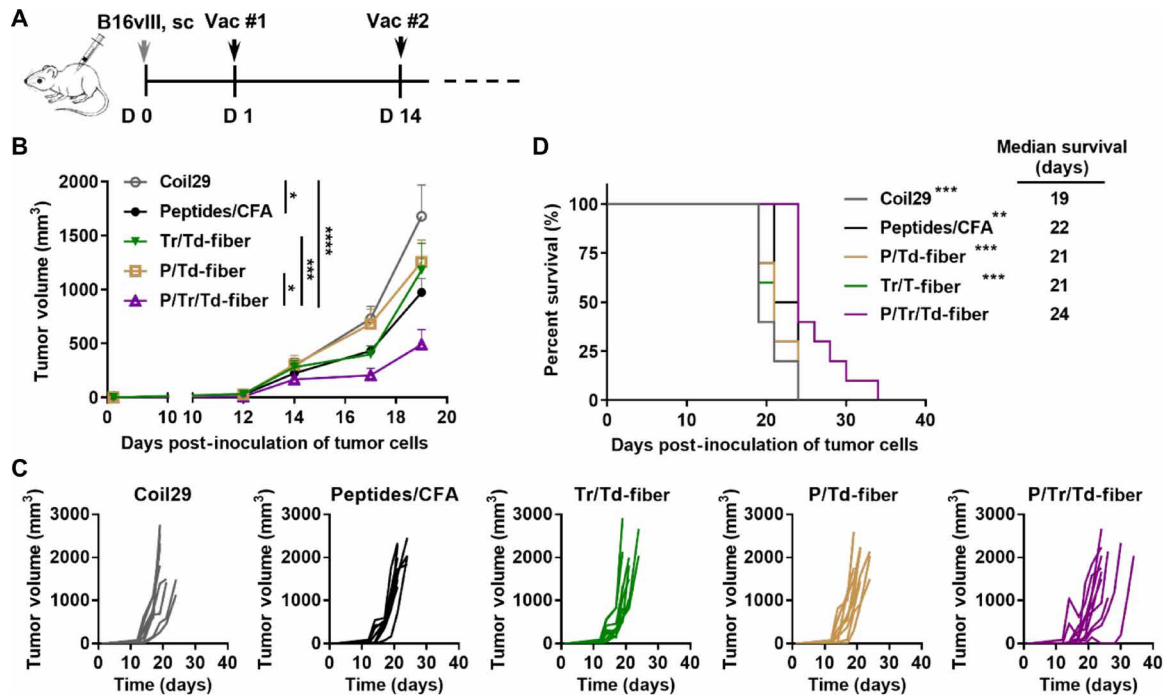
Fig. 5. Multiepitope nanofiber vaccine inhibited the growth of established B16vIII tumors. (**A**) C57BL/6 mice were inoculated on the flank subcutaneously with 1×10^5 B16vIII tumor cells and then treated with indicated nanofiber formulations on days 1 and 14. (**B**) Tumor growth was measured over time (*$P < 0.05$, ***$P < 0.001$, and ****$P < 0.0001$, multiple comparison by two-way ANOVA with Tukey test, $N = 10$). (**C**) Individual tumor growth curves. (**D**) Overall survival of tumor-bearing mice and median survival (**$P < 0.01$ and ***$P < 0.001$ compared to P/Tr/Td-fiber group by log-rank test, $N = 10$).

and no cell lysis was observed when tumor cells were incubated with PBS sera. In addition, only low levels of cytotoxicity were recorded when B16F10 cells were used as target in the same assays. This confirmed that anti-PEPvIII antibodies could induce EGFRvIII receptor–specific ADCC activities against B16vIII cells. To determine whether aCD47 antibodies could enhance the observed ADCC activities, we cocultured B16vIII and NK cells in the presence of sera from mice immunized with P/Td-fibers, P/Tr/Td-fibers, CFA, or PBS, with the addition of either aCD47 antibodies or isotype controls (Fig. 6A and fig. S8). Sera from all three immunization groups mediated tumor lysis by NK cells without aCD47 antibodies. Moreover, 32.1 and 33.6% of tumor cells were killed by NK cells when incubated with sera from P/Td-fiber group and P/Tr/Td-fiber group, respectively, higher than 22.2% in the CFA group. The difference is likely caused by the significantly higher concentration of PEPvIII-specific IgG antibodies elicited by nanofiber vaccines. When compared with the isotype corresponding group, the addition of aCD47 antibodies significantly elevated the ADCC activities for both the P/Td-fiber (38.5%, $P = 0.0067$) and P/Tr/Td-fiber groups (40.0%, $P < 0.0001$), suggesting that aCD47 can potentially enhance the antitumor ADCC activities induced by nanofiber vaccines. The CFA group also had a comparable fold change (fig. S11A). It is worth noting that aCD47 antibodies alone can mediate ADCC cell killing, consistent with previous reports (*54*), which could partly contribute to the enhancement by aCD47 observed in the PBS groups. Because of the low baseline level of ADCC activity in the PBS group when treated with isotype controls, the addition of aCD47 yielded significantly higher fold change in the PBS group (fig. S11A).

To examine serum antibody–mediated ADCP activity, bone marrow–derived macrophages (BMDMs) were labeled with cell-trace far red and seeded in a nontreated 96-well plate before cocultured with sera-treated CFSE-labeled B16vIII cells in an E:T ratio of 2:1 with or without aCD47 (Fig. 6B and figs. S9 and S11B). CFSE+F4/80+ cells were defined as macrophages that phagocytosed B16vIII target cells, and the percentage of CFSE+ macrophages is defined as ADCP activity (*59*). Without the addition of aCD47, only sera from the P/Td-fiber group mediated a statistically significant increase of ADCP (5.22%) when compared to the PBS-treated group (3.52%). The addition of aCD47 antibodies significantly enhanced ADCP activities, roughly a twofold change in the P/Td-fiber group and a 2.5-fold change in the P/Tr/Td-fiber group, as compared to the isotype controls (fig. S11B). A smaller boost by aCD47 was also observed in the CFA group, but no significant ADCP activity was induced by aCD47 alone. Moreover, vaccine-induced sera antibodies mediated significantly higher ADCP activities against B16vIII than against B16F10, suggesting that antibody binding to EGFRvIII receptors is important for the observed ADCP activity by BMDM (fig. S10). Therefore, aCD47 antibodies improved both ADCC and ADCP against B16vIII cells, mediated by EGFRvIII-specific antibodies elicited by nanofiber vaccines.

We lastly evaluated the therapeutic effect of aPD-L1 on the cellular cytotoxicity mediated by vaccine-induced T cells (Fig. 6C and fig. S11C). We isolated splenocytes from vaccine-immunized mice and cocultured them with CFSE-labeled B16vIII cells at an E:T ratio of 10:1 for 20 hours. The resulting B16vIII cell viabilities are defined as cytotoxic T lymphocyte (CTL) activity. The addition of aPD-L1 antibodies led to about a twofold increase in cellular toxicity for all
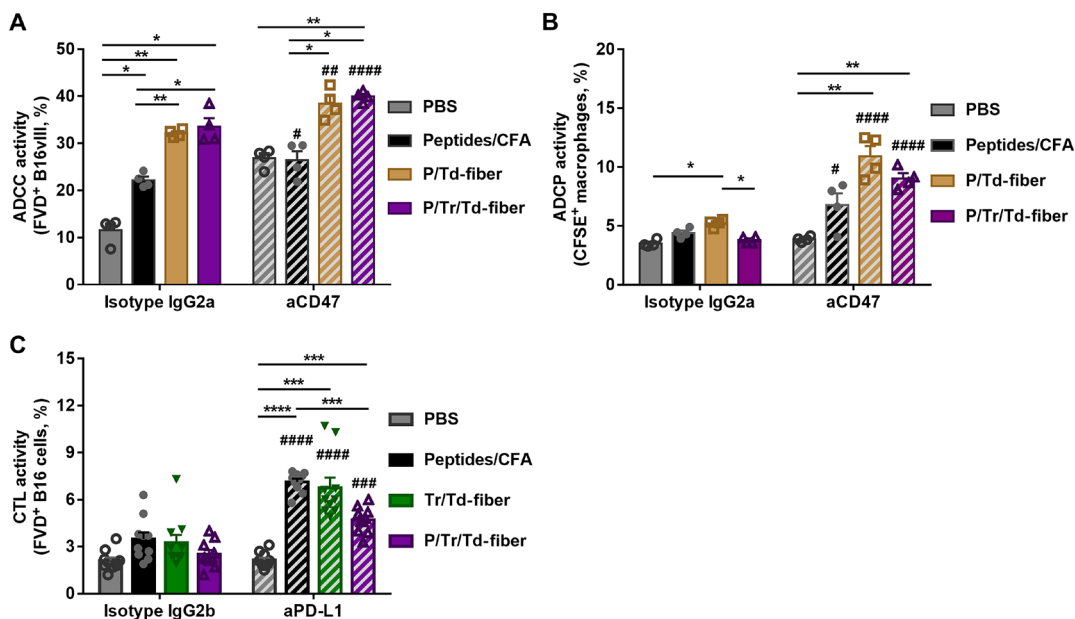
Fig. 6. Blockade antibodies enhanced serum antibody–mediated antitumor ADCC, ADCP, and T cell–mediated tumor lysis in vitro. (**A**) Anti-CD47 blockade antibodies enhanced in vitro ADCC activities mediated by PEPvIII-specific sera antibodies. B16vIII cells were incubated with mouse NK cells with an E:T ratio of 1:1 in the presence of sera from indicated groups, in addition to aCD47 or isotype IgG2a antibodies. The percentage of dead B16vIII cells is defined as ADCC activity. (**B**) Anti-CD47 blockade antibodies promoted in vitro ADCP activities mediated by PEPvIII-specific sera antibodies. B16vIII cells were incubated with BMDM with an E:T ratio of 2:1 in the presence of mouse sera from indicated groups and aCD47 or isotype control. The percentage of B16vIII-phagocytozed macrophages is defined as ADCP activity and was assessed after 5-hour incubation. (**C**) Anti–PD-L1 blockade antibodies improved in vitro cytotoxic responses mediated by T cells induced by vaccines. CFSE-labeled B16vIII cells were cocultured with splenocytes from immunized mice in Fig. 3A with an E:T ratio of 10:1 in the presence of aPD-L1 or IgG2b isotype control. The viability of B16vIII was assessed after 20-hour incubation as CTL activity [*$P < 0.05$, **$P < 0.01$, ***$P < 0.001$, and ****$P < 0.0001$ determined within either isotype control or blockade antibody group, by multiple comparison using one-way ANOVA with Tukey test; #$P < 0.05$, ##$P < 0.01$, ###$P < 0.001$, and ####$P < 0.0001$ between blockade antibody and isotype groups within each corresponding serum group by multiple comparison using two-way ANOVA with Bonferroni test; for (A) and (B), $N = 4$; for (C), $N = 10$].

three immunization groups, but no activity enhancement was observed for the PBS group or isotype control (fig. S11C). This confirms that vaccination can induce cytotoxic T cell responses and that aPD-L1 antibodies can significantly enhance the cellular toxicity mediated by these T cells.

Because aCD47 and aPD-L1 antibodies improved therapeutic effects in vitro, we then sought to further improve the therapeutic effect of P/Tr/Td-fiber vaccine by coadministering the combination blockade antibodies (aPD-L1 and aCD47). We treated B16vIII tumor–bearing mice with P/Tr/Td-fiber vaccines and blockade antibodies at predetermined time points (Fig. 7A). As expected, the vaccine/blockade antibodies combination generated therapeutic synergy and significantly improved tumor inhibition and long-term survival over the blockade antibodies group and P/Tr/Td-fiber vaccine alone group (Fig. 7, B to D). This result confirms that blockade antibodies can further improve a vaccine-induced therapeutic effect potentially by enhancing T cell–mediated cellular cytotoxicity and antibody-mediated cytotoxicity, namely, ADCC and ADCP.

DISCUSSION
There is mounting evidence that endogenous antitumor humoral responses provide substantial benefit for tumor treatment. A high level of antitumor antibodies is associated with positive prognosis in several human cancers (*1–5*). Comprehensive genomic sequencing has also indicated that the presence of NK cells and B cell isotype switching within the tumor microenvironment are associated with

prolonged survival (*6*). However, even with seroconversion, humoral cancer vaccines often provide little therapeutic improvement in cancer patients, indicating that a combination therapy capable of more fully engaging immunity may be necessary to maximize the therapeutic effect of antibodies (*21, 28*). Several recent clinical trials demonstrated that the presence of B cells and lymphoid tertiary structures in tumor tissues enhanced cancer immunotherapy, suggesting that a synergy between B cells and T cells can facilitate cancer immunotherapy (*60–62*). This is corroborated by a preclinical study where combination between TAA-specific antibodies and T cell vaccines generated outstanding therapeutic efficacy in established tumors (*9*). Therefore, a cancer vaccine that induces both humoral and cellular responses against different cancer antigens could potentially realize the therapeutic potential of antibodies and be more effective in tumor treatment.

We previously established two modular self-assembling nanofiber systems, the α-helical peptides used here (Coil29) and β-sheet fibrillizing peptides (Q11). Both systems can carry multiple epitopes and induce CD4$^+$ T cell help for enhanced humoral responses (*30, 35*). The modularity of this type of platform also affords flexibility for modifying surface chemistry to modulate immunogenicity via a variety of routes, including mucosally (*63, 64*). Moreover, unadjuvanted Coil29 nanofibers elicit antibody responses with both higher concentrations and better quality, compared to several commercial adjuvants and Q11 nanofibers (*31*). Here, we exploited the immunogenicity and modularity of the Coil29 platform to design a multiepitope nanofiber cancer vaccine (P/Tr/Td-fiber) carrying CD4$^+$
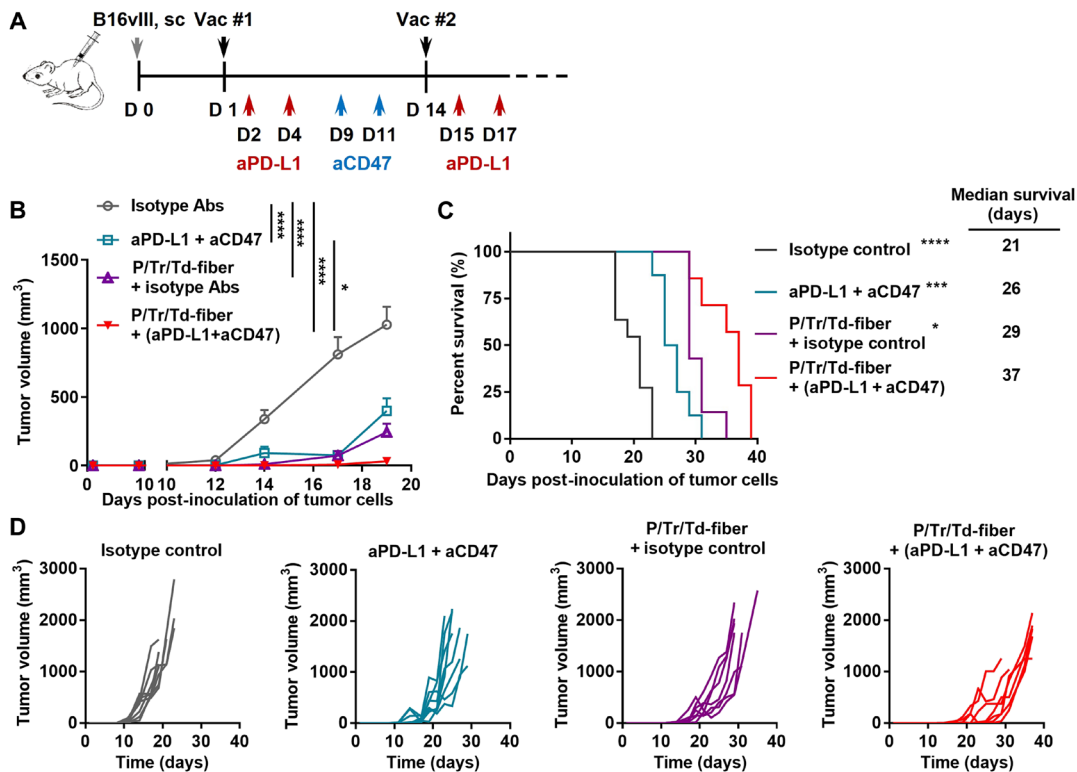
Fig. 7. Blockade antibodies potentiated tumor suppression by multiepitope nanofiber vaccines. (**A**) C57BL/6 mice were inoculated on the flank subcutaneously with 1×10^5 B16vIII tumor cells and then treated with multiepitope nanofiber vaccines on days 1 and 14, in combination with isotype IgG2a or aCD47 antibodies (50 μg) that were administered intratumorally on days 9 and 11 (blue arrow) and isotype IgG2b or aPD-L1 antibodies (100 μg) that were administered intraperitoneally on days 2, 4, 15, and 17 (red arrow). (**B**) Tumor growth was measured over time (*$P < 0.05$ and ****$P < 0.0001$ by multiple comparison using two-way ANOVA with Tukey test, $N = 10$). (**C**) Overall survival of tumor-bearing mice and median survival (*$P < 0.05$, ***$P < 0.001$, and ****$P < 0.0001$ compared to P/Tr/Td-fiber group by log-rank test, $N = 10$). (**D**) Individual tumor growth curves.

T cell epitopes, CD8^{+} T cell epitopes, and B cell epitopes to induce antitumor humoral and cellular responses. Consistent with previous findings, the co-assembled Coil29 nanofibers carry all three different epitopes (Fig. 1) and stimulate strong antigen-specific antitumor humoral responses (Fig. 2A) along with CD4^{+} and CD8^{+} T cell responses (Fig. 3). In comparison, despite the strong adjuvanticity, the CFA/peptide emulsion was only effective in inducing T cell responses and produced antibodies with considerably lower titers compared to nanofiber vaccines. By comparison, Coil29 nanofibers were much more capable of raising simultaneous responses against multiple different peptide epitopes.

A key advantage of tumor antigen-specific antibody responses is the ability to leverage innate immunity for cancer treatment (*12*), whereas typical CD8^{+} T cell vaccines primarily rely on adaptive immunity. We found that P/Tr/Td-fiber vaccines induced IgG antibodies binding specifically to EGFRvIII, a tumor-associated receptor (Fig. 2B), and in turn, this mediated effective in vitro tumoricidal ADCC and ADCP responses (Fig. 6, A and B), confirming that nanofiber vaccines induce functional antibody responses and can engage NK cells and macrophages to inhibit tumor growth. Moreover, we also found that cellular responses elicited by Coil29 nanofibers were as effective as those induced by CFA emulsions in a CTL assay (Fig. 6C). The vaccine-induced multifaceted responses allowed for the engagement of both adaptive immunity and innate immunity and exhibited therapeutic enhancement in both prophylactic and

therapeutic models, over either humoral or cellular responses alone (Figs. 4 and 5). In addition, the P/Tr/Td-fiber vaccine showed greater therapeutic efficacy than CFA emulsions, demonstrating the ability of Coil29 nanofibers to elicit responses against multiple peptide antigens. These findings suggest that the humoral and cellular immune responses elicited by the P/Tr/Td-fiber vaccines synergize and generate enhanced therapeutic effects.

To attenuate the suppressive tumor microenvironment and improve the antitumor effect of the P/Tr/Td-fiber vaccines, we designed a triple combination treatment with both the P/Tr/Td-fiber vaccine and two checkpoint blockade antibodies, aCD47 and aPD-L1. The aCD47 antibody, a recently established phagocytosis checkpoint blockade antibody (*56*), enhances direct tumor killing by macrophages and NK cells (*54*, *55*), promotes DC antigen presentation (*65*), and requires adaptive immunity for durable antitumor responses (*66*). Consistent with previous reports, we found that aCD47 antibodies potentiated both BMDM-mediated ADCP and NK-mediated ADCC. This tumoricidal effect was largely dependent on the presence of vaccine-induced PEPvIII-specific antibodies, demonstrating the therapeutic synergy between blockade antibodies and antitumor antibodies (Fig. 6, A and B). Moreover, the addition of aPD-L1 antibodies also improved direct killing by T cells induced by the vaccines. Consistent with previous reports (*66*–*68*), the combination of aCD47 and aPD-L1 alone showed moderate antitumor efficacy. However, this triple combination therapy showed marked improvement

in both tumor inhibition and mouse survival over the antibodies or vaccines alone, demonstrating a promising therapeutic synergy enabled by the multi-epitope nanofiber vaccine (Fig. 7).

There are a few limitations for the present study. One important shortcoming of this study is that the therapeutic effect was significantly limited by the timing of humoral responses governed by the intrinsic B cell developmental dynamics (69), as it takes multiple weeks for antibody concentrations to reach maxima. To evaluate the potential therapeutic effect of vaccine-induced antibodies, we immunized mice 1 day after tumor inoculation. To minimize the confounding factors that might be caused by this accelerated treatment regimen, we included the Coil29/CpG group to confirm that the observed therapeutic effects were generated by tumor epitope–specific immunity. Nevertheless, the presence of low levels of antibodies, when combined with CD8$^+$ T cell responses, still showed inhibitory effects in the therapeutic model, indicating the importance of antibody responses, even submaximal (Fig. 5). Future work may benefit from a focus on designing an immunization strategy to induce high levels of antibody responses in a shorter time frame. Further, while the CD8$^+$ T cell responses induced by the P/Tr/Td-fiber vaccine were similar to the CFA-adjuvanted group, they were suboptimal for tumor treatments. This could potentially be caused by inefficient trafficking to draining lymph nodes by the micrometer-sized assemblies (70). To potentially overcome this shortcoming, we recently demonstrated that the unique assembling mechanism of the α-helical Coil29 nanofiber system affords more control over the length of the assemblies and can be used to modulate lymph node trafficking to enhance cellular responses (70). This strategy could potentially be adapted for the multiepitope nanofiber vaccine reported here to improve its therapeutic efficacy. We selected CFA owing to its strong immunostimulatory effects for peptide antigens (45). However, considering differences in the adjuvanting mechanisms of CFA and CpG, we compared T cell and antibody responses between the Peptides/CFA and Peptides/CpG groups, finding that both adjuvants were similarly effective in eliciting T cell and antibody responses against the epitopes investigated (fig. S12). Also, while CpG is an effective adjuvant in mice due to the promiscuous nature of TLR9 expression in murine B cells and T cells, its effect is limited in humans (71). Future translational studies may consider poly(I:C) (polyinosinic-polycytidylic acid) as an alternative adjuvant choice (72). Despite these limitations, the nanofiber vaccine illustrates a supramolecular strategy to leverage vaccine-induced humoral responses, in combination with CD8$^+$ T cell responses, for improved cancer treatment. This combinatorial strategy could be potentially applicable for a range of different cancers including glioblastoma (22) or breast cancer (26), with important considerations for future combinatorial cancer vaccine therapies.

In summary, we demonstrate that Coil29 nanofibers are a useful platform for simultaneously delivering combinations of peptide epitopes for B cells, CD4$^+$ T cells, and CD8$^+$ T cells. The P/Tr/Td-fiber vaccine raises EGFRvIII receptor–specific antibody responses superior to CFA emulsions and simultaneously generates cellular responses comparable to CFA emulsions. The simultaneous anti-tumor humoral and cellular responses allowed P/Tr/Td-fiber vaccines to engage both innate and adaptive immunity, yielding significant tumor inhibition in both prophylactic and therapeutic B16vIII tumor models, relative to either responses alone or CFA emulsions. The therapeutic efficacy of the P/Tr/Td-fiber vaccine could be further improved by dual checkpoint blockade antibodies, aCD47 and

aPD-L1. The notable improvement in efficacy afforded by P/Tr/Td-fiber vaccines over other single-target vaccines underscores the critical role of endogenous antitumor antibodies. Our findings suggest a multiepitope vaccine design strategy and shed light on a triple combination strategy between vaccines and blockade antibodies (aCD47 and aPD-L1) to fully engage innate and adaptive immunity for improved efficacy of cancer immunotherapies.

MATERIALS AND METHODS
Peptides
All peptides were synthesized using Fmoc solid-phase chemistry on a CEM Liberty Blue microwave-assisted synthesizer and purified with high-performance liquid chromatography (HPLC) and matrix-assisted laser desorption/ionization–mass spectrometry (MALDI-MS). Biotinylated peptides were synthesized on-resin by reacting Biotin-ONp (33755-53-2, Novabiochem) with amine-terminated peptides in a threefold excess overnight in N,N'-dimethylformamide (DMF). DBCO was conjugated with peptides by reacting DBCO-NHS Ester (A133-100, Click Chemistry Tools) with amine-terminated peptide on-resin overnight in DMF in the presence of diisopropylethylamine (DIEA). TAMRA-labeled peptides were prepared on-resin by reacting 5(6)-TAMRA (AS-81124, Anaspec Inc.) in a threefold excess with the addition of N,N'-diisopropylcarbodiimide (DIC) and 6-chloro-1-hydroxybenzotriazole (HOBt-Cl). Alexa Fluor 750–labeled peptides were prepared on-resin by reacting Alexa Fluor 750 NHS Ester (A37575, Thermo Fisher Scientific) with amine-terminated peptides in the presence of DIEA overnight in DMF.

Immunization formulations
To prepare peptide nanofiber immunization solutions, lyophilized peptides were weighed and mixed at predetermined molar ratios (PEPvIII-Coil29:Td-Coil29:Coil29 = 1:1:1 for P/Td-fiber, Trp2-Coil29:Td-Coil29:Coil29 = 1:1:1 for Tr/Td-fiber, and PEPvIII-Coil29:Trp2-Coil29:Td-Coil29 = 1:1:1 for P/Tr/Td-fiber). Mixed peptide powders were then dissolved at 8 mM in sterile 10 mM acetate buffer (pH 4) and incubated overnight at 4°C. The peptide solutions were subsequently mixed with CpG [ODN 1826 (type B), AdipoGen] and diluted to yield a final peptide concentration of 2 mM and CpG concentration of 500 μg/ml in 1× PBS. The mixed solutions were incubated for 3 hours at room temperature before immunizations. Other modified peptide nanofibers were prepared in the same fashion before usage. For CFA/IFA peptide emulsions, all three epitope peptides (PEPvIII, Trp2, and Td) were mixed at a molar ratio of 1:1:1, dissolved at 4 mM in sterile water, then mixed with an equal volume of CFA or IFA (Incomplete Freund's Adjuvant), and vortexed for 45 min to yield adjuvanted emulsions with a final total peptide concentration of 2 mM for immunization.

TEM analysis
Nanofiber solutions were prepared as for immunizations, followed by 10-fold dilution to 0.2 mM in 1× PBS. To prepare sample grids for imaging, 5 μl of diluted sample solution was deposited onto 400 mesh carbon copper grids (EMS400-CU, EMS). After 1-min incubation at room temperature, sample grids were washed three times with deionized (DI) water and stained with 2 μl of 1% uranyl acetate for 30 s. Sample grids were air-dried after the excess liquid was blotted away with filter paper. For gold nanoparticle–labeled samples, 5 μl of diluted sample solutions was deposited onto 400-mesh carbon

copper grids for 1-min incubation, followed by DI water. After the excess liquid was blotted away, 5 μl of 5-nm azide-functionalized gold nanoparticles (CK11, Nanopartz) was added onto the grids and incubated for 5 min. The excess liquid was then blotted away, and the grids were rinsed first with the droplets of 1% Tween 1× PBS solution for three times and then with DI water droplets for three times. Subsequently, 5 μl of 10-nm streptavidin-labeled gold nanoparticles (S9059, Sigma-Aldrich) was added to the sample grids for 5-min incubation after excess liquid was blotted away. Last, the excess liquid was blotted away, and the sample grids were washed with 1% Tween solution and DI water and stained with 2 μl of 1% uranyl acetate for 30 s. Sample grids were imaged using FEI Tecnai F30 TEM and analyzed with FEI TEM Imaging and Analysis (TIA) software.

CD analysis
A Bioz PiStar CD spectrometer was used with a 0.1-cm path length quartz cell. Nanofiber solutions were prepared the same way as previously described and were further diluted to 0.1 mM with 1× PBS for analysis. The spectra were collected between 190 and 260 nm with a scanning speed of 0.5 nm s^{-1} and a bandwidth of 0.5 nm. Each spectrum shown was the average of three scans, with the solvent background subtracted.

In vitro antigen presentation
BMDCs were generated after 7-day culture of mouse femur bone marrow in complete RPMI media [RPMI 1640 with L-glutamine, 10 mM Hepes, 50 μM β-mercaptoethanol, 1 mM sodium pyruvate, 1 mM nonessential amino acids, and 10% fetal bovine serum (FBS)] supplemented with Flt3L (10 ng/ml; PHC9411, Life Technologies). To examine T cell epitope presentations, SIINFEKL-fibers (SIINFEKL-Coil29:Coil29 = 1:2), OVA$_{323-339}$-fiber (OVA$_{323-339}$-Coil29:Coil29 = 1:2), and SIINFEKL/OVA$_{323-339}$-fiber (SIINFEKL-Coil29:OVA$_{323-339}$-Coil29:Coil29 = 1:1:1) were prepared in the same way as indicated above. BMDCs were seeded (100,000 cells at 1 M/ml) into 96-well plates and incubated with either nanofibers or peptide epitopes at indicated concentrations for 4 hours at 37°C in a humidified CO$_2$ incubator. The wells were then emptied after 5-min centrifugation at 500g to remove excess peptides, followed by the addition of B3Z cells or DOBW cells (100,000 cells at 1 M/ml) to detect the presentation of SIINFEKL or OVA$_{323-339}$, respectively. Cocultures were incubated for 20 hours at 37°C in a humidified CO$_2$ incubator. To detect SIINFEKL presentation, BMDC/B3Z coculture cells were incubated with 150 μl of CPRG/lysis buffer [0.15 mM chlorophenol red-β-D-galactopyranoside (CPRG), 0.1% Triton X-100, 9 mM MgCl$_2$, and 100 μM β-mercaptoethanol in PBS] at 37°C for 90 min after media were emptied. The absorbance at 570 nm of each well was determined using a microplate reader. To detect OVA$_{323-339}$ presentation, BMDC/DOBW coculture media were collected and measured for the concentration of IL-2 using an IL-2 cytokine enzyme-linked immunosorbent assay (ELISA) kit (55148, BD).

Immunizations
Female C57BL/6NHsd mice (7 to 9 weeks old) were purchased from Harlan Laboratories and housed at the animal facility of Duke University. All animal procedures were performed in accordance with and approved by the Institutional Animal Care and Use Committee of Duke University under protocol #A199-21-09 and #A283-15-11. Mice were anesthetized under isoflurane and immunized subcutaneously with 100 μl of indicated solutions (200 nmol each peptide epitope per mouse, 50 μl at each shoulder) and boosted with half-doses (100 nmol

each peptide epitope per mouse 25 μl at each shoulder) at indicated time points when required. For cellular uptake experiments, 100 μl of indicated nanofiber solutions was administered intraperitoneally. After 4 hours, 1 ml of intraperitoneal lavage was collected from each mouse and the cells were purified after centrifugation for subsequent analysis.

Blood samples were collected from submandibular vein to analyze for either PBMCs or epitope-specific sera antibodies. To isolate PBMCs, 100 μl of whole-blood samples was treated with 1 ml of ammonium-chloride-potassium (ACK) lysis buffer (A1049201, Thermo Fisher Scientific) for three times and subsequently washed with 2 ml of flow buffer (2% FBS in 1× PBS) via centrifugation (500g, 5 min). The purified PBMCs were subsequently stained for flow cytometry analysis. IgG ELISA and subclass phenotyping is performed in streptavidin (85878, Sigma-Aldrich)–treated 96-well plates against biotin-PEPvIII peptides, using alkaline phosphatase–conjugated detection antibodies for total IgG, IgG1, IgG2b, IgG2c, or IgG3 (115-055-071, 115-055-205, 115-055-207, 115-055-208, and 115-055-209, respectively, Jackson ImmunoResearch).

Tumor model
Vaccinated mice were challenged 14 days after their last immunization by subcutaneous injection of 1×10^5 B16vIII cells into the right flank of recipient mice. Tumor growth was monitored every other day, and the tumor volume was calculated as follows: volume = length × width^2 × 0.52. Animals were euthanized when the masses reached 1.5 cm in diameter, when tumor volume reached 2000 mm^3, or when ulceration occurred. For the therapeutic tumor model, mice were inoculated with 1×10^5 B16vIII cells in 200 μl of 1× PBS into the right flank. Vaccinations were given 1 day after tumor inoculation, and booster immunizations were given 14 days after primary vaccination. For combinatorial immunotherapy, anti-mouse PD-L1 (100 μg per mouse, clone 10F.9G2, BioXCell) or IgG2b isotype control (100 μg per mouse, clone LTF-2, BioXCell) was administered intraperitoneally on indicated days, and anti-mouse CD47 (50 μg per mouse, clone MIAP301, BioXCell) or IgG2a isotype control (50 μg per mouse, clone 2A3, BioXCell) was administered intratumorally on indicated days. Tumor growth was determined as described above.

Flow cytometry
To detect antigen uptake, peritoneal cells were stained for Fixable Viability Dye (FVD; L34963, Thermo Fisher Scientific), CD45 (BV605, clone 30-F11, BioLegend), F4/80 [peridinin chlorophyll protein (PerCP)–Cy5.5, clone BM8, BioLegend], CD19 [phycoerythrin (PE)–Cy7, clone 1D3, BD], CD11c [allophycocyanin (APC), clone N418, BioLegend], and MHCII (FITC, clone M5/114.15.2, BioLegend). Individual cell populations were defined as follows: macrophages, FVD$^-$CD45$^+$F4/80$^+$; B cells, FVD$^-$CD45$^+$CD19$^+$; DCs, FVD$^-$CD45$^+$CD11c$^+$MHCII$^+$. PEPvIII antigen–internalized cells are defined as PE$^+$ cells, and Trp2 antigen–internalized cells are defined as APC-Cy7$^+$ cells.

To determine cell frequencies in lymph nodes, lymph nodes were dissected 7 days after the last immunization. Single-cell suspensions were prepared by pressing lymph nodes through a 70-μm cell strainer. Half of the cells were stained for FVD, CD45, CD19, GL7 (FITC, clone GL7, BD), and Fas (PE-Cy7, clone Jo2, BD). GC B cells were defined as FVD$^-$CD45$^+$CD19$^+$GL7$^+$Fas$^+$. The rest of the cells were initially stained for biotinylated CXCR5 (clone SPRCL5, Thermo Fisher Scientific) at 1:50 antibody dilution for 40 min and then stained for FVD, CD3e (bV605, clone 145-2C11, BD), CD4 (FITC,

clone GK1.5, BioLegend), CD44 (APC-Cy7, clone IM7, BD), PD-1 (APC, clone RMP1-30, BD), and streptavidin-PE (405203, BioLegend). T_{FH} cells were defined as FVD⁻CD3e⁺CD4⁺CD44⁺PD-1⁺CXCR5⁺.

To determine antigen-specific CD8⁺ T cell frequencies, PBMCs were initially stained for APC-labeled Trp2 tetramers (National Institutes of Health tetramer core) at 2.5 μg/ml for 1 hour at 37°C in a humidified CO_2 incubator and then stained for FVD, CD3e, CD4, and CD8a (PE-Cy7, clone 53-6.7, BD). Trp2-specific CD8⁺ T cells were defined as FVD⁻CD3e⁺CD4⁻CD8⁺Trp2⁺.

Cells were stained at a 1:200 antibody dilution unless otherwise stated. Flow cytometry was performed using BD Canto II instrument and analyzed using FlowJo software (FlowJo 10.7.1).

Enzyme-linked immunospot

To evaluate epitope-specific T cell responses, splenocytes were collected from vaccinated mice 7 days after their last immunizations. After splenocytes were purified with lympholyte-M (CL5031, Cedarlane), 0.25 million splenocytes were plated in each well of a 96-well ELISPOT plate (Millipore, MSIPS4510), in 200 μl per well. The cells were either left unstimulated as negative control or stimulated with peptides (1×10^{-3} mM Trp2, or 1×10^{-3} mM Td) or ConA (positive control, C5275, Sigma) for 20 hours at 37°C in a humidified CO_2 incubator. IFNγ ELISPOT pairs (551881, BD), streptavidin–alkaline phosphatase (3310-10-1000, Mabtech), and Sigmafast BCIP/NBT substrate (B5655, Sigma) were used to detect and develop antigen-specific spots. Plates were enumerated by ZellNet Consulting using a Zeiss KS ELISPOT system.

Antibody-dependent cellular cytotoxicity

To expand NK cells, splenocytes were first purified with lympholyte-M and then cultured in a 15-cm tissue culture–treated petri dish at a density of 2 M/ml in the complete RPMI media supplemented with IL-2 (1000 U/ml; RP-8605, Thermo Fisher Scientific). IL-2–containing culture media were changed every 2 days, and nonadherent cells were harvested after 12-day culture. NK cell phenotype was confirmed using flow cytometry as CD45⁺CD11c⁻CD19⁻NK1.1⁺. To determine ADCC activities, B16vIII or B16F10 cells were first labeled with CFSE (C34554, Thermo Fisher Scientific) and then seeded onto 96-well plates at 2×10^4 cells per well. After overnight culture at 37°C in a humidified CO_2 incubator, the cells were incubated with diluted sera pooled from naïve mice or immunized mice within the same treatment group at room temperature for 30 min. Sera were diluted 10-, 50-, and 250-fold in complete RPMI media to demonstrate the serum antibody dependence. In all other assays, sera were diluted 10-fold in complete RPMI media. After 30-min incubation with sera, the same number of NK cells was added onto B16vIII or B16F10 cell media to yield the final E:T ratio of 1:1. When aCD47 antibodies were used, aCD47 (7 μg/ml) or isotype control antibodies were added into the coculture. The viability of tumor cells (CFSE⁺) was determined after 7-hour coculture via FVD staining using flow cytometry.

Antibody-dependent cellular phagocytosis

To generate BMDMs, after treatment with ACK lysis buffer, mouse femur bone marrow cells were seeded at a density of 0.5 M/ml in non–cell culture–treated 15-cm petri dish and cultured in complete RPMI media supplemented with macrophage colony-stimulating factor (20 ng/ml; 416-ML-010/CF, R&D Systems) for 7 days. The adherent cells were then detached via treatment with Accutase (A1110501, Thermo Fisher Scientific) for subsequent coculture assays. Macrophage phenotype was confirmed using flow cytometry as F4/80⁺. To determine ADCP activities, BMDMs were labeled with CellTrace Yellow (C34567, Thermo Fisher Scientific) and seeded onto a non–tissue culture–treated 96-well plate at 0.5 M/ml density in 10% IMDM (Iscove's Modified Dulbecco's Medium) media (IMDM media with 10% FBS). Twenty hours later, BMDM culture media were changed from 10% IMDM to FBS-free IMDM and cells were incubated 37°C in a humidified CO_2 incubator for 2 hours before coculture assay. CFSE-labeled B16vIII or B16F10 cells were incubated with 50-fold diluted sera as described above. After IMDM media were emptied, the opsonized tumor cells were added onto BMDM wells to yield the final E:T ratio of 2:1. aCD47 and isotype control antibodies (7 μg/ml) were used as indicated. The tumor cell–phagocytosed BMDM cells were defined as CFSE⁺F4/80⁺.

CTL assay

CFSE-labeled B16vIII cells were seeded onto 96-well plates at 0.05 M/ml and stimulated with IFNγ (500 U/ml; 575302, BioLegend) for 20 hours. Splenocytes from immunized mice were harvested and purified with lympholyte M, before coculture with B16vIII cells at a final E:T ratio of 10:1 in a humidified CO_2 incubator. After 48-hour coculture, cells were suspended after treatment of Accutase and stained for FVD to assess the viability of tumor cells. When aPD-L1 antibodies were used, aPD-L1 or isotype control antibodies (40 μg/ml) were added into the coculture.

Statistical analysis

Statistical analyses were performed using GraphPad Prism 8. Statistical analysis for each experiment was specified in the figure captions. All values are reported as means ± SEM, with sample sizes indicated in figure captions. Sample sizes were chosen based on pilot experiments and previously published results in the literature. Comparisons of multiple groups at a single time point were performed with one-way analysis of variance (ANOVA), and comparisons of multiple groups over time were performed by using two-way ANOVA tests. Experiments were not performed in a blinded fashion. No samples were excluded from analysis.

SUPPLEMENTARY MATERIALS

REFERENCES AND NOTES

1. D. A. Bolotin, S. Poslavsky, A. N. Davydov, F. E. Frenkel, L. Fanchi, O. I. Zolotareva, S. Hemmers, E. V. Putintseva, A. S. Obraztsova, M. Shugay, R. I. Ataullakhanov, A. Y. Rudensky, T. N. Schumacher, D. M. Chudakov, Antigen receptor repertoire profiling from RNA-seq data. *Nat. Biotechnol.* **35**, 908–911 (2017).

2. M. D. Iglesia, J. S. Parker, K. A. Hoadley, J. S. Serody, C. M. Perou, B. G. Vincent, Genomic analysis of immune cell infiltrates across 11 tumor types. *J. Natl. Cancer Inst.* **108**, djw144 (2016).

3. O. I. Isaeva, G. V. Sharonov, E. O. Serebrovskaya, M. A. Turchaninova, A. R. Zaretsky, M. Shugay, D. M. Chudakov, Intratumoral immunoglobulin isotypes predict survival in lung adenocarcinoma subtypes. *J. Immunother. Cancer* **7**, 279 (2019).

4. M. Reuschenbach, M. von Knebel Doeberitz, N. Wentzensen, A systematic review of humoral immune responses against tumor antigens. *Cancer Immunol. Immunother.* **58**, 1535–1544 (2009).

5. G. V. Sharonov, E. O. Serebrovskaya, D. V. Yuzhakova, O. V. Britanova, D. M. Chudakov, B cells, plasma cells and antibody repertoires in the tumour microenvironment. *Nat. Rev. Immunol.* **20**, 294–307 (2020).

6. X. Hu, J. Zhang, J. Wang, J. Fu, T. Li, X. Zheng, B. Wang, S. Gu, P. Jiang, J. Fan, X. Ying, J. Zhang, M. C. Carroll, K. W. Wucherpfennig, N. Hacohen, F. Zhang, P. Zhang, J. S. Liu, B. Li, X. S. Liu, Landscape of B cell immunity and related immune evasion in human cancers. *Nat. Genet.* **51**, 560–567 (2019).

7. E. Van Cutsem, C. H. Kohne, E. Hitre, J. Zaluski, C. R. C. Chien, A. Makhson, G. D'Haens, T. Pinter, R. Lim, G. Bodoky, J. K. Roh, G. Folprecht, P. Ruff, C. Stroh, S. Tejpar, M. Schlichting, J. Nippgen, P. Rougier, Cetuximab and chemotherapy as initial treatment for metastatic colorectal cancer. *N. Engl. J. Med.* **360**, 1408–1417 (2009).

8. C. A. Hudis, Trastuzumab - Mechanism of action and use in clinical practice. *N. Engl. J. Med.* **357**, 39–51 (2007).

9. K. D. Moynihan, C. F. Opel, G. L. Szeto, A. Tzeng, E. F. Zhu, J. M. Engreitz, R. T. Williams, K. Rakhra, M. H. Zhang, A. M. Rothschilds, S. Kumari, R. L. Kelly, B. H. Kwan, W. Abraham, K. Hu, N. K. Mehta, M. J. Kauke, H. Suh, J. R. Cochran, D. A. Lauffenburger, K. D. Wittrup, D. J. Irvine, Eradication of large established tumors in mice by combination immunotherapy that engages innate and adaptive immune responses. *Nat. Med.* **22**, 1402–1410 (2016).

10. K. D. Wittrup, Antitumor antibodies can drive therapeutic T cell responses. *Trends Cancer* **3**, 615–620 (2017).

11. Y. Carmi, M. H. Spitzer, I. L. Linde, B. M. Burt, T. R. Prestwood, N. Perlman, M. G. Davidson, J. A. Kenkel, E. Segal, G. V. Pusapati, N. Bhattacharya, E. G. Engleman, Allogeneic IgG combined with dendritic cell stimuli induce antitumour T-cell immunity. *Nature* **521**, 99–104 (2015).

12. A. M. Scott, J. D. Wolchok, L. J. Old, Antibody therapy of cancer. *Nat. Rev. Cancer* **12**, 278–287 (2012).

13. C. H. Chung, B. Mirakhur, E. Chan, Q. Le, J. Berlin, M. Morse, B. A. Murphy, S. M. Satinover, J. Hosen, D. Mauro, R. J. Slebos, Q. W. Zhou, D. Gold, T. Hatley, D. J. Hicklin, T. A. E. Platts-Mills, Cetuximab-induced anaphylaxis and IgE specific for galactose-α-1,3-galactose. *N. Engl. J. Med.* **358**, 1109–1117 (2008).

14. N. F. Ponde, M. Lambertini, E. de Azambuja, Twenty years of anti-HER2 therapy-associated cardiotoxicity. *Esmo Open* **1**, e000073 (2016).

15. Z. Hu, P. A. Ott, C. J. Wu, Towards personalized, tumour-specific, therapeutic vaccines for cancer. *Nat. Rev. Immunol.* **18**, 168–182 (2018).

16. U. Sahin, E. Derhovanessian, M. Miller, B. P. Kloke, P. Simon, M. Löwer, V. Bukur, A. D. Tadmor, U. Luxemburger, B. Schrors, T. Omokoko, M. Vormehr, C. Albrecht, A. Paruzynski, A. N. Kuhn, J. Buck, S. Heesch, H. Katharina, F. Muller, I. Ortseifer, I. Vogler, E. Godehardt, S. Attig, R. Rae, A. Breitkreuz, C. Tolliver, M. Suchan, G. Martic, A. Hohberger, P. Sorn, J. Diekmann, J. Ciesla, O. Waksmann, A. K. Burck, M. Witt, M. Zillgen, A. Rothermel, B. Kasemann, D. Langer, S. Bolte, M. Diken, S. Kreiter, R. Nemecek, C. Gebhardt, S. Grabbe, C. Höller, J. Utikal, C. Huber, C. Loquai, Ö. Türeci, Personalized RNA mutanome vaccines mobilize poly-specific therapeutic immunity against cancer. *Nature* **547**, 222–226 (2017).

17. P. A. Ott, Z. Hu, D. B. Keskin, S. A. Shukla, J. Sun, D. J. Bozym, W. Zhang, A. Luoma, A. Giobbie-Hurder, L. Peter, C. Chen, O. Olive, T. A. Carter, S. Li, D. J. Lieb, T. Eisenhaure, E. Gjini, J. Stevens, W. J. Lane, I. Javeri, K. Nellaiappan, A. M. Salazar, H. Daley, M. Seaman, E. I. Buchbinder, C. H. Yoon, M. Harden, N. Lennon, S. Gabriel, S. J. Rodig, D. H. Barouch, J. C. Aster, G. Getz, K. Wucherpfennig, D. Neuberg, J. Ritz, E. S. Lander, E. F. Fritsch, N. Hacohen, C. J. Wu, An immunogenic personal neoantigen vaccine for patients with melanoma. *Nature* **547**, 217–221 (2017).

18. R. Kuai, L. J. Ochyl, K. S. Bahjat, A. Schwendeman, J. J. Moon, Designer vaccine nanodiscs for personalized cancer immunotherapy. *Nat. Mater.* **16**, 489–496 (2017).

19. L. Scheetz, K. S. Park, Q. Li, P. R. Lowenstein, M. G. Castro, A. Schwendeman, J. J. Moon, Engineering patient-specific cancer immunotherapies. *Nat. Biomed. Eng.* **3**, 768–782 (2019).

20. J. Schuster, R. K. Lai, L. D. Recht, D. A. Reardon, N. A. Paleologos, M. D. Groves, M. M. Mrugala, R. Jensen, J. M. Baehring, A. Sloan, G. E. Archer, D. D. Bigner, S. Cruickshank, J. A. Green, T. Keler, T. A. Davis, A. B. Heimberger, J. H. Sampson, A phase II, multicenter trial of rindopepimut (CDX-110) in newly diagnosed glioblastoma: The ACT III study. *Neuro Oncol.* **17**, 854–861 (2015).

21. M. Weller, N. Butowski, D. Tran, L. Recht, M. Lim, H. Hirte, L. Ashby, L. Mechtler, S. Goldlust, F. Iwamoto, J. Drappatz, D. O'Rourke, M. Wong, G. Finocchiaro, J. Perry, W. Wick, Y. He, T. Davis, R. Stupp, J. Sampson, ATIM-03. ACT IV: An international, double-blind, phase 3 trial of rindopepimut in newly diagnosed, EGFRvIII-expressing glioblastoma. *Neuro Oncol.* **18**, vi17–vi18 (2016).

22. D. C. Binder, E. Ladomersky, A. Lenzen, L. J. Zhai, K. L. Lauing, S. D. Otto-Meyer, R. V. Lukas, D. A. Wainwright, Lessons learned from rindopepimut treatment in patients with EGFRvIII-expressing glioblastoma. *Transl. Cancer Res.* **7**, S510–S513 (2018).

23. J. H. Sampson, A. B. Heimberger, G. E. Archer, K. D. Aldape, A. H. Friedman, H. S. Friedman, M. R. Gilbert, J. E. Herndon, R. E. McLendon, D. A. Mitchell, D. A. Reardon, R. Sawaya, R. J. Schmittling, W. M. Shi, J. J. Vredenburgh, D. D. Bigner, Immunologic escape after prolonged progression-free survival with epidermal growth factor receptor variant III peptide vaccination in patients with newly diagnosed glioblastoma. *J. Clin. Oncol.* **28**, 4722–4729 (2010).

24. M. Weller, P. Roth, M. Preusser, W. Wick, D. A. Reardon, M. Platten, J. H. Sampson, Vaccine-based immunotherapeutic approaches to gliomas and beyond. *Nat. Rev. Neurol.* **13**, 363–374 (2017).

25. D. M. O'Rourke, M. P. Nasrallah, A. Desai, J. J. Melenhorst, K. Mansfield, J. J. D. Morrissette, M. Martinez-Lage, S. Brem, E. Maloney, A. Shen, R. Isaacs, S. Mohan, G. Plesa, S. F. Lacey, J.-M. Navenot, Z. Zheng, B. L. Levine, H. Okada, C. H. June, J. L. Brogdon, M. V. Maus, A single dose of peripherally infused EGFRvIII-directed CAR T cells mediates antigen loss and induces adaptive resistance in patients with recurrent glioblastoma. *Sci. Transl. Med.* **9**, eaaa0984 (2017).

26. H. M. Stern, Improving treatment of HER2-positive cancers: Opportunities and challenges. *Sci. Transl. Med.* **4**, 127rv122 (2012).

27. D. L. Wheeler, E. F. Dunn, P. M. Harari, Understanding resistance to EGFR inhibitors—Impact on future treatment strategies. *Nat. Rev. Clin. Oncol.* **7**, 493–507 (2010).

28. G. Curigliano, G. Romieu, M. Campone, T. Dorval, L. Duck, J.-L. Canon, C. Roemer-Becuwe, M. Roselli, S. Neciosup, W. Burny, A. Callegaro, P. M. de Sousa Alves, J. Louahed, V. Brichard, F. F. Lehmann, A phase I/II trial of the safety and clinical activity of a HER2-protein based immunotherapy for treating women with HER2-positive metastatic breast cancer. *Breast Cancer Res. Treat.* **156**, 301–310 (2016).

29. R. J. Malonis, J. R. Lai, O. Vergnolle, Peptide-based vaccines: Current progress and future challenges. *Chem. Rev.* **120**, 3210–3229 (2020).

30. Y. Wu, P. K. Norberg, E. A. Reap, K. L. Congdon, C. N. Fries, S. H. Kelly, J. H. Sampson, V. P. Conticello, J. H. Collier, A supramolecular vaccine platform based on α-helical peptide nanofibers. *ACS Biomater. Sci. Eng.* **3**, 3128–3132 (2017).

31. Y. Wu, S. H. Kelly, L. Sanchez-Perez, J. H. Sampson, J. H. Collier, Comparative study of α-helical and β-sheet self-assembled peptide nanofiber vaccine platforms: Influence of integrated T-cell epitopes. *Biomater. Sci.* **8**, 3522–3535 (2020).

32. E. H. Egelman, C. Xu, F. DiMaio, E. Magnotti, C. Modlin, X. Yu, E. Wright, D. Baker, V. P. Conticello, Structural plasticity of helical nanotubes based on coiled-coil assemblies. *Structure* **23**, 280–289 (2015).

33. A. B. Heimberger, L. E. Crotty, G. E. Archer, K. R. Hess, C. J. Wikstrand, A. H. Friedman, H. S. Friedman, D. D. Bigner, J. H. Sampson, Epidermal growth factor receptor VIII peptide vaccination is efficacious against established intracerebral tumors. *Clin. Cancer Res.* **9**, 4247–4254 (2003).

34. Z. Xu, S. Ramishetti, Y.-C. Tseng, S. Guo, Y. Wang, L. Huang, Multifunctional nanoparticles co-delivering Trp2 peptide and CpG adjuvant induce potent cytotoxic T-lymphocyte response against melanoma and its lung metastasis. *J. Control. Release* **172**, 259–265 (2013).

35. R. R. Pompano, J. Chen, E. A. Verbus, H. Han, A. Fridman, T. McNeely, J. H. Collier, A. S. Chong, Titrating T-cell epitopes within self-assembled vaccines optimizes CD4+ helper T cell and antibody outputs. *Adv. Healthc. Mater.* **3**, 1898–1908 (2014).

36. P. Novy, M. Quigley, X. P. Huang, Y. P. Yang, CD4 T cells are required for CD8 T cell survival during both primary and memory recall responses. *J. Immunol.* **179**, 8243–8251 (2007).

37. J. Borst, T. Ahrends, N. Babala, C. J. M. Melief, W. Kastenmuller, CD4+ T cell help in cancer immunology and immunotherapy. *Nat. Rev. Immunol.* **18**, 635–647 (2018).

38. A. Zeltins, J. West, F. Zabel, A. El Turabi, I. Balke, S. Haas, M. Maudrich, F. Storni, P. Engeroff, G. T. Jennings, A. Kotecha, D. I. Stuart, J. Foerster, M. F. Bachmann, Incorporation of tetanus-epitope into virus-like particles achieves vaccine responses even in older recipients in models of psoriasis, Alzheimer's and cat allergy. *Npj Vaccines* **2**, 30 (2017).

39. D. M. Pardoll, The blockade of immune checkpoints in cancer immunotherapy. *Nat. Rev. Cancer* **12**, 252–264 (2012).

40. M. Y. Feng, W. Jiang, B. Y. S. Kim, C. C. Zhang, Y. X. Fu, I. L. Weissman, Phagocytosis checkpoints as new targets for cancer immunotherapy. *Nat. Rev. Cancer* **19**, 568–586 (2019).

41. R. Majeti, M. P. Chao, A. A. Alizadeh, W. W. Pang, S. Jaiswal, K. D. Gibbs, N. van Rooijen, I. L. Weissman, CD47 Is an adverse prognostic factor and therapeutic antibody target on human acute myeloid leukemia stem cells. *Cell* **138**, 286–299 (2009).

42. K. Nagy-Smith, P. J. Beltramo, E. Moore, R. Tycko, E. M. Furst, J. P. Schneider, Molecular, local, and network-level basis for the enhanced stiffness of hydrogel networks formed from coassembled racemic peptides: Predictions from Pauling and Corey. *ACS Cent. Sci.* **3**, 586–597 (2017).

43. J. H. Collier, J. S. Rudra, J. Z. Gasiorowski, J. P. Jung, Multi-component extracellular matrices based on peptide self-assembly. *Chem. Soc. Rev.* **39**, 3413–3424 (2010).

44. C. Schliehe, C. Redaelli, S. Engelhardt, M. Fehlings, M. Mueller, N. van Rooijen, M. Thiry, K. Hildner, H. Weller, M. Groettrup, CD8−dendritic cells and macrophages cross-present poly(D,L-lactate-co-glycolate) acid microsphere-encapsulated antigen In vivo. *J. Immunol.* **187**, 2112–2121 (2011).

45. H. F. Stils Jr., Adjuvants and antibody production: Dispelling the myths associated with Freund's complete and other adjuvants. *ILAR J.* **46**, 280–293 (2005).

46. C. L. B. Millan, R. Weeratna, A. M. Krieg, C. A. Siegrist, H. L. Davis, CpG DNA can induce strong Th1 humoral and cell-mediated immune responses against hepatitis B surface antigen in young mice. *Proc. Natl. Acad. Sci. U.S.A.* **95**, 15553–15558 (1998).

47. H. Shirota, D. Tross, D. M. Klinman, CpG oligonucleotides as cancer vaccine adjuvants. *Vaccine* **3**, 390–407 (2015).

48. U. Ohto, T. Shibata, H. Tanji, H. Ishida, E. Krayukhina, S. Uchiyama, K. Miyake, T. Shimizu, Structural basis of CpG and inhibitory DNA recognition by Toll-like receptor 9. *Nature* **520**, 702–705 (2015).

49. G. D. Victora, M. C. Nussenzweig, Germinal centers. *Annu. Rev. Immunol.* **30**, 429–457 (2012).

50. S. Crotty, T follicular helper cell biology: A decade of discovery and diseases. *Immunity* **50**, 1132–1148 (2019).

51. N. S. Joshi, W. Cui, A. Chandele, H. K. Lee, D. R. Urso, J. Hagman, L. Gapin, S. M. Kaech, Inflammation directs memory precursor and short-lived effector CD8+ T cell fates via the graded expression of T-bet transcription factor. *Immunity* **27**, 281–295 (2007).

52. M. Binnewies, E. W. Roberts, K. Kersten, V. Chan, D. F. Fearon, M. Merad, L. M. Coussens, D. I. Gabrilovich, S. Ostrand-Rosenberg, C. C. Hedrick, R. H. Vonderheide, M. J. Pittet, R. K. Jain, W. P. Zou, T. K. Howcroft, E. C. Woodhouse, R. A. Weinberg, M. F. Krummel, Understanding the tumor immune microenvironment (TIME) for effective therapy. *Nat. Med.* **24**, 541–550 (2018).

53. M. P. Chao, A. A. Alizadeh, C. Tang, J. H. Myklebust, B. Varghese, S. Gill, M. Jan, A. C. Cha, C. K. Chan, B. T. Tan, C. Y. Park, F. F. Zhao, H. E. Kohrt, R. Malumbres, J. Briones, R. D. Gascoyne, I. S. Lossos, R. Levy, I. L. Weissman, R. Majeti, Anti-CD47 antibody synergizes with Rituximab to promote phagocytosis and eradicate non-Hodgkin lymphoma. *Cell* **142**, 699–713 (2010).

54. X. W. Zhao, E. M. van Beek, K. Schornagel, H. Van der Maaden, M. Van Houdt, M. A. Otten, P. Finetti, M. Van Egmond, T. Matozaki, G. Kraal, D. Birnbaum, A. van Elsas, T. W. Kuijpers, F. Bertucci, T. K. van den Berg, CD47–signal regulatory protein-α (SIRPα) interactions form a barrier for antibody-mediated tumor cell destruction. *Proc. Natl. Acad. Sci. U.S.A.* **108**, 18342–18347 (2011).

55. D. Tseng, J.-P. Volkmer, S. B. Willingham, H. Contreras-Trujillo, J. W. Fathman, N. B. Fernhoff, J. Seita, M. A. Inlay, K. Weiskopf, M. Miyanishi, I. L. Weissman, Anti-CD47 antibody–mediated phagocytosis of cancer by macrophages primes an effective antitumor T-cell response. *Proc. Natl. Acad. Sci. U.S.A.* **110**, 11103–11108 (2013).

56. R. Advani, I. Flinn, L. Popplewell, A. Forero, N. L. Bartlett, N. Ghosh, J. Kline, M. Roschewski, A. LaCasce, G. P. Collins, T. Tran, J. Lynn, J. Y. Chen, J. P. Volkmer, B. Agoram, J. Huang, R. Majeti, I. L. Weissman, C. H. Takimoto, M. P. Chao, S. M. Smith, CD47 blockade by Hu5F9-G4 and rituximab in non-Hodgkin's lymphoma. *N. Eng. J. Med.* **379**, 1711–1721 (2018).

57. K. Weiskopf, N. S. Jahchan, P. J. Schnorr, S. Cristea, A. M. Ring, R. L. Maute, A. K. Volkmer, J.-P. Volkmer, J. Liu, J. S. Lim, D. Yang, G. Seitz, T. Nguyen, D. Wu, K. Jude, H. Guerston, A. Barkal, F. Trapani, J. George, J. T. Poirier, E. E. Gardner, L. A. Miles, E. de Stanchina, S. M. Lofgren, H. Vogel, M. M. Winslow, C. Dive, R. K. Thomas, C. M. Rudin, M. van de Rijn, R. Majeti, K. C. Garcia, I. L. Weissman, J. Sage, CD47-blocking immunotherapies stimulate macrophage-mediated destruction of small-cell lung cancer. *J. Clin. Invest.* **126**, 2610–2620 (2016).

58. M. Yamashita, S. Kitano, H. Aikawa, A. Kuchiba, M. Hayashi, N. Yamamoto, K. Tamura, A. Hamada, A novel method for evaluating antibody-dependent cell-mediated cytotoxicity by flowcytometry using cryopreserved human peripheral blood mononuclear cells. *Sci. Rep.* **6**, 19772 (2016).

59. L. Kamen, S. Myneni, C. Langsdorf, E. Kho, B. Ordonia, T. Thakurta, K. Zheng, A. Song, S. Chung, A novel method for determining antibody-dependent cellular phagocytosis. *J. Immunol. Methods* **468**, 55–60 (2019).

60. B. A. Helmink, S. M. Reddy, J. Gao, S. Zhang, R. Basar, R. Thakur, K. Yizhak, M. Sade-Feldman, J. Blando, G. Han, V. Gopalakrishnan, Y. Xi, H. Zhao, R. N. Amaria, H. A. Tawbi, A. P. Cogdill, W. Liu, V. S. LeBleu, F. G. Kugeratski, S. Patel, M. A. Davies, P. Hwu, J. E. Lee, J. E. Gershenwald, A. Lucci, R. Arora, S. Woodman, E. Z. Keung, P.-O. Gaudreau, A. Reuben, C. N. Spencer, E. M. Burton, L. E. Haydu, A. J. Lazar, R. Zapassodi, C. W. Hudgens, D. A. Ledesma, S. Ong, M. Bailey, S. Warren, D. Rao, O. Krijgsman, E. A. Rozeman, D. Peeper, C. U. Blank, T. N. Schumacher, L. H. Butterfield, M. A. Zelazowska, K. M. McBride, R. Kalluri, J. Allison, F. Petitprez, W. H. Fridman, C. Sautès-Fridman, N. Hacohen, K. Rezvani, P. Sharma, M. T. Tetzlaff, L. Wang, J. A. Wargo, B cells and tertiary lymphoid structures promote immunotherapy response. *Nature* **577**, 549–555 (2020).

61. F. Petitprez, A. de Reyniès, E. Z. Keung, T. W.-W. Chen, C.-M. Sun, J. Calderaro, Y.-M. Jeng, L.-P. Hsiao, L. Lacroix, A. Bougoüin, M. Moreira, G. Lacroix, I. Natario, J. Adam, C. Lucchesi, Y. H. Laizet, M. Toulmonde, M. A. Burgess, V. Bolejack, D. Reinke, K. M. Wani, W.-L. Wang, A. J. Lazar, C. L. Roland, J. A. Wargo, A. Italiano, C. Sautès-Fridman, H. A. Tawbi, W. H. Fridman, B cells are associated with survival and immunotherapy response in sarcoma. *Nature* **577**, 556–560 (2020).

62. R. Cabrita, M. Lauss, A. Sanna, M. Donia, M. Skaarup Larsen, S. Mitra, I. Johansson, B. Phung, K. Harbst, J. Vallon-Christersson, A. van Schoiack, K. Lövgren, S. Warren, K. Jirström, H. Olsson, K. Pietras, C. Ingvar, K. Isaksson, D. Schadendorf, H. Schmidt, L. Bastholt, A. Carneiro, J. A. Wargo, I. M. Svane, G. Jönsson, Tertiary lymphoid structures improve immunotherapy and survival in melanoma. *Nature* **577**, 561–565 (2020).

63. Y. Wen, A. Waltman, H. Han, J. H. Collier, Switching the immunogenicity of peptide assemblies using surface properties. *ACS Nano* **10**, 9274–9286 (2016).

64. S. H. Kelly, Y. Wu, A. K. Varadhan, E. J. Curvino, A. S. Chong, J. H. Collier, Enabling sublingual peptide immunization with molecular self-assemblies. *Biomaterials* **241**, 119903 (2020).

65. X. J. Liu, Y. Pu, K. Cron, L. F. Deng, J. Kline, W. A. Frazier, H. R. Xu, H. Peng, Y. X. Fu, M. M. Xu, CD47 blockade triggers T cell–mediated destruction of immunogenic tumors. *Nat. Med.* **21**, 1209–1215 (2015).

66. J. T. Sockolosky, M. Dougan, J. R. Ingram, C. C. M. Ho, M. J. Kauke, S. C. Almo, H. L. Ploegh, K. C. Garcia, Durable antitumor responses to CD47 blockade require adaptive immune stimulation. *Proc. Natl. Acad. Sci. U.S.A.* **113**, E2646–E2654 (2016).

67. S. Lian, R. Xie, Y. Ye, Y. Lu, Y. Cheng, X. Xie, S. Li, L. Jia, Dual blockage of both PD-L1 and CD47 enhances immunotherapy against circulating tumor cells. *Sci. Rep.* **9**, 4532 (2019).

68. X. Liu, L. Liu, Z. Ren, K. Yang, H. Xu, Y. Luan, K. Fu, J. Guo, H. Peng, M. Zhu, Y. X. Fu, Dual targeting of innate and adaptive checkpoints on tumor cells limits immune evasion. *Cell Rep.* **24**, 2101–2111 (2018).

69. J. G. Cyster, C. D. C. Allen, B cell responses: Cell interaction dynamics and decisions. *Cell* **177**, 524–540 (2019).

70. C. N. Fries, Y. Wu, S. H. Kelly, M. Wolf, N. L. Votaw, S. Zauscher, J. H. Collier, Controlled lengthwise assembly of helical peptide nanofibers to modulate CD8+ T-cell responses. *Adv. Mater.* **32**, 2003310 (2020).

71. C. Bode, G. Zhao, F. Steinhagen, T. Kinjo, D. M. Klinman, CpG DNA as a vaccine adjuvant. *Expert Rev. Vaccines* **10**, 499–511 (2011).

72. J. De Waele, T. Verhezen, S. van der Heijden, Z. N. Berneman, M. Peeters, F. Lardon, A. Wouters, E. L. J. M. Smits, A systematic review on poly(I:C) and poly-ICLC in glioblastoma: Adjuvants coordinating the unlocking of immunotherapy. *J. Exp. Clin. Cancer Res.* **40**, 213 (2021).